UNIVERSITY OF CALIFORNIA,
IRVINE

Structural, Electrical and Optical Characterization of Thiol Treated PbTe Thin Films Infilled by Alumina ALD

DISSERTATION
submitted in partial satisfaction of the requirements
for the degree of
DOCTOR OF PHILOSOPHY
in
Chemical and Biochemical Engineering
by
Juliette Alyssa Hunter Micone

Dissertation Committee:
Professor Matt Law, Chair
Professor Enrique Lavernia
Professor Reginald Penner

2018

Dedication

I would like to dedicate my thesis to my family for their continued support with all of my endeavors. Their strength of will and love for me will always be wanted and needed.

Table of Contents

Page

List of Figures

Page

Acknowledgements

I sincerely acknowledge my advisor, Matt Law, for his continued support, kindness, and guidance throughout my graduate career. His expertise in his field knows no bounds and his efforts to build me up as a better scientist and person will always be appreciated. I am grateful to the entire Law Lab, both past and present, which provide knowledge, support and someone to laugh and cry with.

I would like to thank Professors Reginald Penner and Enrique Lavernia for serving on my thesis committee. They provided advice and encouragement toward the development of this body of work and improving my confidence in technical speaking.

I acknowledge the support I received from my advisor, Matt Law through funding provided by Department of Energy, Energy Frontier Research Centers (EFRC); Center for Advanced Solar Photophysics (CASP) and Defense Advanced Research Projects Agency (DARPA).

The members of the LEXI, IMRI, and INRF/BION facilities at UC Irvine have provided immeasurable amounts of expertise towards developing my technical skills. I never would have imagined that I could operate such high level equipment and work in cleanroom environments before beginning my graduate career. I thank you for your efforts to maintain all of the equipment and providing advice toward characterizing my materials.

The members of the Matt Law Lab deserve considerable thanks for providing me support as colleagues and as friends through our research meetings, frustrations with maintaining equipment in the lab, and sharing joys and hardships through our graduate career. I especially thank Dr. Mark Gibbs, Dr. Jason Tolentino, and Dr. Brandon Mercado who trained me when I first joined the lab. I also thank my undergraduate, Glen Junor, for his hard work on examining the stability of the PbTe QDs in solution. Furthermore, I thank Claire Gilpin, Kan Fu, Chao Yi, Alex Abelson, Benjamin Adam Wells, Caroline Qian, Zhongyue Luan, Yash Gargasya, and Trenton Salk.

Lastly, I wish to thank my mother and father, Julie and Frank Micone, for always supporting and believing in me and my brother, Brett Micone, for providing both welcoming and unwelcoming distractions. I love you all. Thank you for everything.

Curriculum Vitae

Juliette A. Micone

EDUACATION

Doctor of Philosophy in Chemical and Biochemical Engineering 2018
University of California, Irvine

Bachelor of Science in Chemical Engineering 2012
University of California, San Diego

RESEARCH EXPERIENCE

Graduate Research Assistant, Matt Law Lab 2012─2018
University of California, Irvine

Research Assistant, Joanna McKittrick Lab 2010─2012
University of California, San Diego

PUBLICATIONS

1. C. Yi, **J. Micone**, K. Fu, A. Ableson, I. Tran, and M. Law. "Approaching Background-Limited Performance (BLIP) in Extended Short-Wavelength Infrared (XSWIR) Quantum Dot Photodetectors through Interface Engineering," (in press)

2. J.K. Han, M. E. Hannah, A. Piquette, **J. Micone**. G. A. Hirata, J. B. Talbot, K. C. Mishra, and J. McKittrick, "Europium-activated barium/strontium silicates for near-UV light emitting diode applications," J. Lumin. 133. 184-187 (2013).

Abstract of the Dissertation

Structural, Electrical and Optical Characterization of Thiol Treated PbTe Thin Films Infilled by Alumina ALD

By

Juliette Alyssa Hunter Micone

Doctor of Philosophy in Chemical and Biochemical Engineering

Univeristy of California, Irvine, 2018

Professor Matt Law, Chair

PbTe quantum dots have demonstrated material handling difficulties arising due to its high reactivity which leads to poor stability, synthetic yields and electronic characteristics. These problems arise even in glovebox environments, where aggressive surface oxidation degrades the material and contribute to the p-channel behavior of thiol treated field effect transistors (FET) which are characterized by low FET mobilities, high carrier concentrations and non-gateable devices. The high reactivity limits the use of typical nucleation assisting precursors which improve nanocrystal formation in PbSe and PbS, but unfortunately lead to rapid, uncontrolled growth of PbTe nanocrystals. The application of ALD (atomic layer deposition) to PbTe films creates new opportunities for study. It scavenges and passivates surface states and some surface oxides that have formed during the ligand exchange and allows the creation of gateable n-channel FET devices with electron mobilities of ~1cm^2/V s and indefinite stability. The poor stability was substantiated through comparison with PbSe quantum dots using UV-Vis

spectroscopy. This thesis will discuss the general theory of quantum dots and initial work on PbTe field effect transistors treated with thiols and infilled with alumina atomic layer deposition.

Chapter 1: Introduction and Background

Introduction and Motivation

It is well understood that current energy demands on Earth will continue to rise well past our lifetimes. This is a cause for concern as fossil fuel use will inevitably diminish due to the lack of resources, concerns for global warming, and a more environmentally conscience populace that, in a simple example, choose electric or fuel cell cars over gasoline powered ones. This necessitates major initiatives in research to find alternatives that are able to fill in the "energy gap" that fossil fuels will leave behind. Many technologies such as solar, wind turbines, and hydropower dams already exist in order to address the energy issue. All of these alternative energy resources, though, have some shortcomings associated with them. They include fundamental problems such as limitations on large scale implementation, efficiencies too low, or fabrication costs too high to make it enticing and advantageous enough to immediately switch over to a society solely powered by renewable resources.

When compared to other renewables, the use of the sun as a resource offers a source of clean, unlimited energy that has potential to satisfy the world's energy needs. Currently, the world total energy consumption is about 18TW annually.[1] This is because the sun shines down on the Earth with a power of 174,000 TW, providing the amount of energy every hour that

humankind uses every year[2]. Therefore, only a fraction of that energy needs to be collected to accommodate our energy needs. With current solar panel materials and efficiencies, the cost and amount of large area solar panels needed to obtain that amount of energy is too high and covering significant portions of land with solar panels can impact plant and wildlife. An approach to tackle this is to create solar technologies with higher efficiencies, novel designs, cheaper materials, and fabrication methods that can harness light across the entire solar spectrum.

Understanding and utilizing the photovoltaic effect is paramount to begin to tackle solar as a solution to our energy needs. Solar energy is harvested through photovoltaics and solar thermal technologies. Photovoltaic devices, such as solar cells, utilize the photovoltaic effect where a material, typically semiconductors, generates voltage or electrical current upon exposure to light. This is done when a photon with energy greater than the band gap of the semiconductor, is absorbed and excites an electron within the valence band and promotes it to the conduction band, thereby creating a hole in the valence band in the process. This electron-hole pair is referred to as an exciton. Photons with energies below the band gap are not absorbed, whereas photons with energies above the band gap are not fully converted to electrical energy because the excess energy is converted into phonon emissions. In p-n junction solar cells, when the electron-hole pair is created in the depletion layer, they are separated by the built-in electric field formed from the shifted Fermi levels of the n and p type semiconductors and then collected for use as electrical energy. The efficiency of this process is limited by several factors. This includes poor capture of the solar spectrum, losses due to phonon emissions, recombination, and trap states within the band gap of the semiconductor.[3,4] The efficiency limit that takes these factors into account is characterized by the Shockley-Quaiser limit which determines the theoretical

maximum efficiency of a p-n junction solar cell. Figure 1 shows this limiting efficiency for a single-junction solar cell under "one-sun" illumination with the standard AM1.5 solar spectrum as a function of band gap; the maximum efficiency occurs for a semiconductor with a band gap of 1.34 eV and is 33.7%.[4] Current research on photovoltaics is divided into three areas. First generation solar cells are comprised of a single p-n junction made from single crystalline silicon. These solar cells have decent efficiencies (~25%) and are the most commercially available. Second generation solar cells are based on thin films of high absorbing materials that can absorb large portions of the solar spectrum and require very little material. Third generation solar cells have the potential to overcome the SQ limit.[5] This approach is aimed to reduce the cost of solar cells by improving their efficiency or power output. Current approaches to create these solar cells include applying multi-junction architectures, up/down conversion, hot-carrier effects, and multiple exciton generation. These areas of research include studies on the perovskite, dye-sensitized, organic, and quantum dot solar cells.[6, 7]

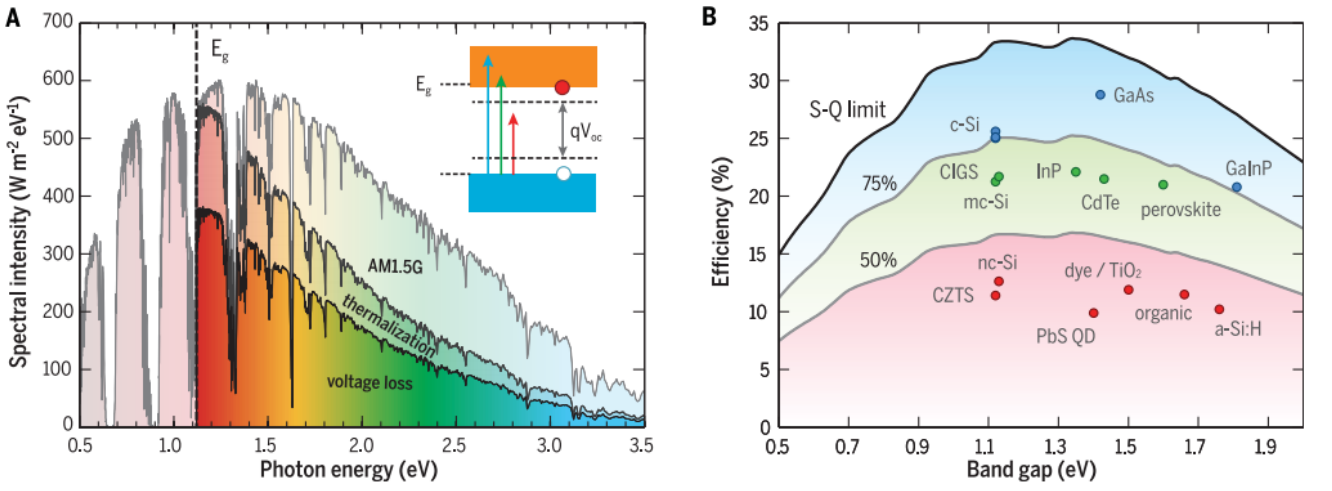

Fig. 1. Fundamental solar cell efficiency limits and present-day records. (**A**) AM1.5 solar spectrum with distinct dips due to molecular absorption in Earth's atmosphere. Photons with energies below the band gap (E_g, dashed black line corresponds to the band gap of Si) are not absorbed, whereas photons with energies above the band gap are not fully converted to electrical energy because of thermalization of charge carriers. The maximum power generated by the cell is limited by voltage loss relative to the band gap voltage. Inset: Electronic band structure with the separation of the quasi-Fermi levels determining the open-circuit voltage V_{oc}. (**B**) Theoretical Shockley-Queisser detailed-balance efficiency limit as a function of band gap (black line) and 75% and 50% of the limit (gray lines). The record efficiencies for different materials are plotted for the corresponding band gaps.

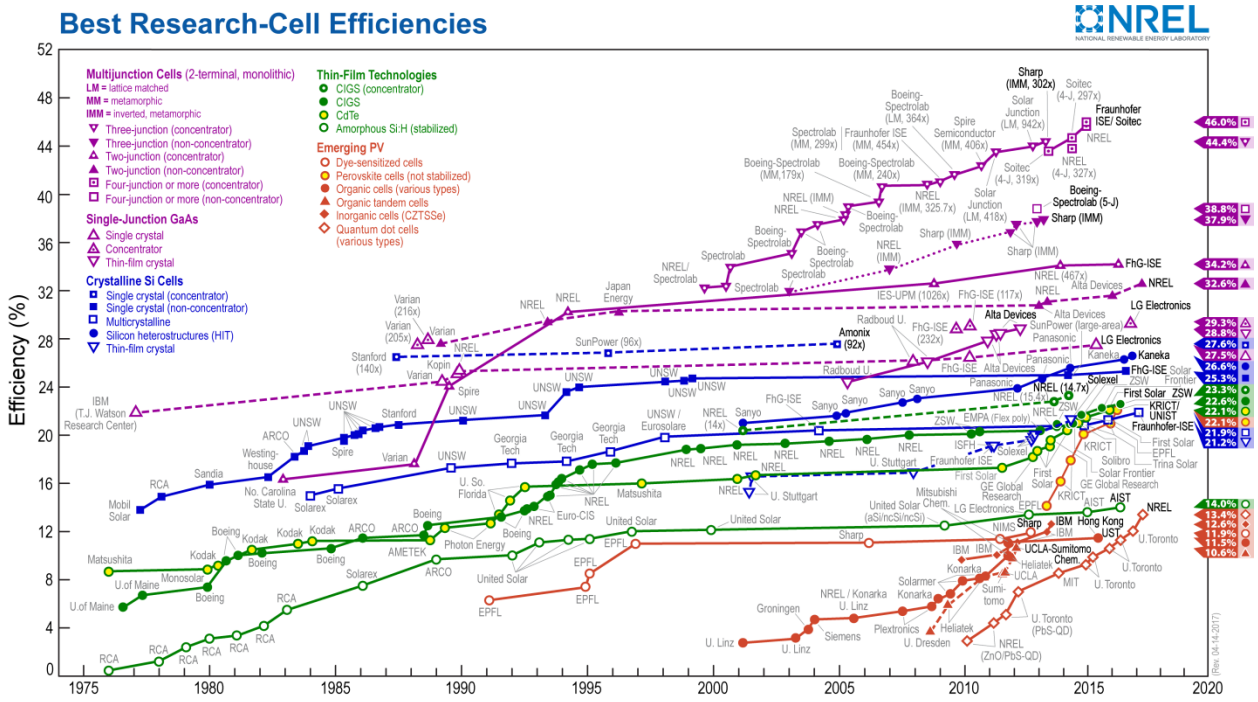

Figure 2. Past and Present Record Efficiencies of Photovoltaic Technologies[8]

The interest in quantum dot materials as a solution to solar is due to the quantum confinement effect that confines charge carriers in all three dimensions of the nanocrystal. When this occurs the energy levels shift from bulk-like to discrete and the materials exhibit properties between that of bulk semiconductors and individual atoms. The most prominent property that results is the tunability of the band gap that can by altered by simply changing the physical size of the nanocrystal. Ideally, this would allow one to create devices covering the entire solar spectrum or specific ranges with a series of different sized quantum dots. Synthesis and film fabrication is relatively simple since they are solution processed materials and can be applied onto nearly any type of substrate or platform with roll-to-roll or spin coating fabrication. These materials are novel nanoscale building blocks that have applications in various electronic and optoelectronic devices including solar, photodetectors, and transistors. The electronic and optical properties of quantum dot devices can be controlled by adjusting their size, surface chemistry,

composition, structure and shape. Lead chalcogenide (PbX, X= S, Se, Te) quantum dots have small band gaps, high absorption coefficients and dielectric constants, and can experience multiple exciton generation (MEG) which has the potential to surpass the SQ limit. Lead telluride quantum dots are of particular interest as it has the largest dielectric constant and Bohr exciton radii of the lead chalcogenides. This leads to stronger quantum confinement, and when fabricated into devices could lead to better electronic coupling, conductivity, and offer greatest potential for efficient MEG due to its slower cooling rate. Studies of lead telluride quantum dot and its surface chemistry not been well explored in literature and gives an opportunity for future work. This paper will discuss the general theory of quantum dots and discuss initial work on PbTe field effect transistors treated with thiols and infilled with atomic layer deposition

Properties of PbX (X= S, Se, Te) Quantum Dots

In bulk semiconductors, the charge carriers are free to move around in the material and have a continuous density of energy states. As the size of the semiconductor decreases, this imparts a physical boundary and restricts the charge carriers' movements as the number of available energy states decreases and the distance between each state increases. Eventually, the semiconductor will become small enough that the charge carriers will "feel" this confinement from the boundaries of the material. The charge carriers are now considered to be quantum confined and have discrete energy levels similar to organic molecules and atoms. The length scale where the carriers feel confined occurs when the size of the nanocrystal is comparable to the Bohr radius of the bound state of the electron and hole called the Bohr exciton radius.[9] If the excitons are confined in three spatial dimensions, the nanocrystal can be referred to as a quantum dot. The size of the Bohr exciton radius of a material is determined by its dielectric constant and the effective masses of the electron and hole. Lead chalcogenide quantum dots, in particular,

have large dielectric constants and small electron and hole effective masses and thus have large Bohr exciton radii with r_{Bohr}= 18, 46, 152 nm for PbS, PbSe, PbTe, respectively.[10] As synthesized PbX (X= S, Se, Te) quantum dots are usually much smaller than their Bohr exciton radii and their carriers experience strong degrees of confinement. This in turn creates strong carrier-carrier interactions due to the increased localization of the coupled electron and hole, and the energy spacings or band gap of the quantum dot can become larger than that of the bandgap of the bulk material.[9] The bandgap of PbX QDs can thus be tuned to cover the entire solar spectrum by simply changing size.

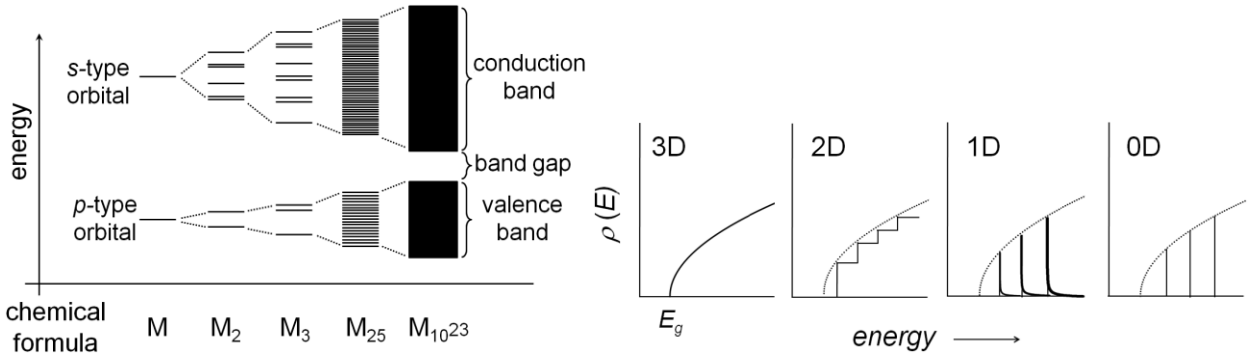

Figure 3 a. (left) Illustration of the formation of energy bands from atomics orbitals. b. (right) Density of Energy States for bulk crystals and structures of reduced dimensionality[11]

The strong confinement demonstrated in PbX QDs results in increased coulombic interactions between carriers. This gives rise to processes such as carrier multiplication within these materials that can potentially surpasses the SQ limit. As discussed earlier, electrons in a semiconductor can be excited across the band gap by absorption of a photon. A photon with energy exceeding the band gap yields an initially hot electron−hole pair with excess energy. This

excess energy can follow several paths. In bulk semiconductors, this excess energy can be dissipated as heat through electron-phonon interactions or Auger processes as the carriers quickly relax to the band edge through the high amount of available states, and thus cannot contribute appreciably to device performance. In QD films, the confinement effect lowers the density of phonon states and slows down the cooling rate of the hot electron. This is most apparent in infrared energy gap PbX QD films, where the incoming photon energy can be much larger than the bandgap of the material and the excess energy of the hot electron can be used to create a second electron-hole pair. In QD films, this process is termed multiple exciton generation as charge carriers exist as bound excitons and not as free carriers. Therefore, devices utilizing MEG must be able to separate and extract the multiple excitons as photocurrent.[12]

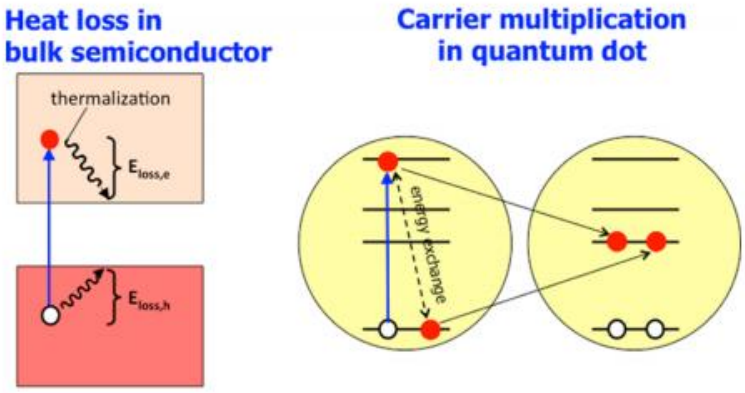

Figure 4. (left) Photoexcition of a bulk semiconductor leads to formation of a hot electron and hole that usually lose their excess energy as heat due to phonon emission. (right) Carrier multiplication in a quantum dot results in excitation of additional electrons across the band gap[12]

Studies of MEG are generally performed utilizing ultrafast techniques such as transient absorption or photoluminescence spectroscopy where a laser pulse of $2E_g$ excites PbX QDs suspended in solution. After photon absorption, the exciton has excess energy and then loses that

energy as they relax to the band edges. The exciton's relaxation to the band edge is measured over time utilizing absorption spectra and the presence of single or biexcitons can be determined based on their different decay rates. It was shown that the onset for MEG occurs at around $2.7E_g$, with PbTe QDs demonstrating the highest quantum yield compared to PbSe and PbS QDs of the same size. The improved MEG was attributed to slower carrier cooling due to better dielectric screening since $\varepsilon = 17, 23, 33$ for PbS, PbSe, PbTe, respectively.[10,13] Another reason for this could be the decreased frequency of longitudinal optical phonons that participate in the cooling process, leading to reduced carrier cooling rates. As the LO phonon frequency decreases and confinement effects increase in heavier lead chalcogenides, it can become smaller than the transition energy between the discrete energy levels in QDs. The carrier cooling process is then likely to require slow multi-phonon instead of fast single-phonon mechanisms, which reduces the overall carrier cooling rate.[14]

PbX QD Synthesis

One of the key advantages of using quantum dots in devices is that they are solution-processed materials that can be easily synthesized and remain colloidally suspended in polar and nonpolar solvents depending on the surface chemistry of the nanocrystal. The most appreciated and commonly used method for quantum dot production is the hot injection method introduced by Murray, Norris, and Bawendi in 1993, when they produced monodisperse cadmium chalcogenide nanocrystals.[15] In the case of metal salt quantum dots (using standard air-free Schlenk line techniques), a cation metal salt, a long-chain coordinating ligand that will act as a surfactant that will bind and passivate the QD surface, and a noncoordinating solvent that does not participate in the reaction are introduced into a round bottom flask. The materials are heated to a desired temperature to form the metal cation complex that will act as one of the precursors

supplying monomers for the nucleation and growth of the quantum dots. In a separate vessel, usually prepared ahead of time, a metal, supplying the anionic precursor to the reaction, is mixed and heated with a phosphine complex and then cooled to room temperature. The round bottom flask containing the metal cation complex is then heated to the desired nucleation temperature. The anionic precursor is rapidly injected into the round bottom immediately forming monomers (Figure 6 (I)) and homogeneously nucleating the nanocrystals (Figure 6 (II)). This nucleation burst occurs when the concentration of monomers in the reaction solution passes a certain threshold and the nanocrystals begin to crystallize as illustrated in Figure 5d [16]. After the injection, the temperature of the reaction drops and further nanocrystal growth occurs due to the continuous supply of monomers onto the nanocrystal surface (Figure 6 (III)) [11]. After a desired growth time is obtained, the reaction is quenched in an ice or water bath and the round bottom is transferred to a glovebox. The surfactant capped nanocrystals are separated from the unreacted precursors and washed through precipitation and centrifugation using polar and nonpolar solvent pairs. The nanocrystals are dried or suspended in clean nonpolar solvents and used for further characterization or film fabrication.

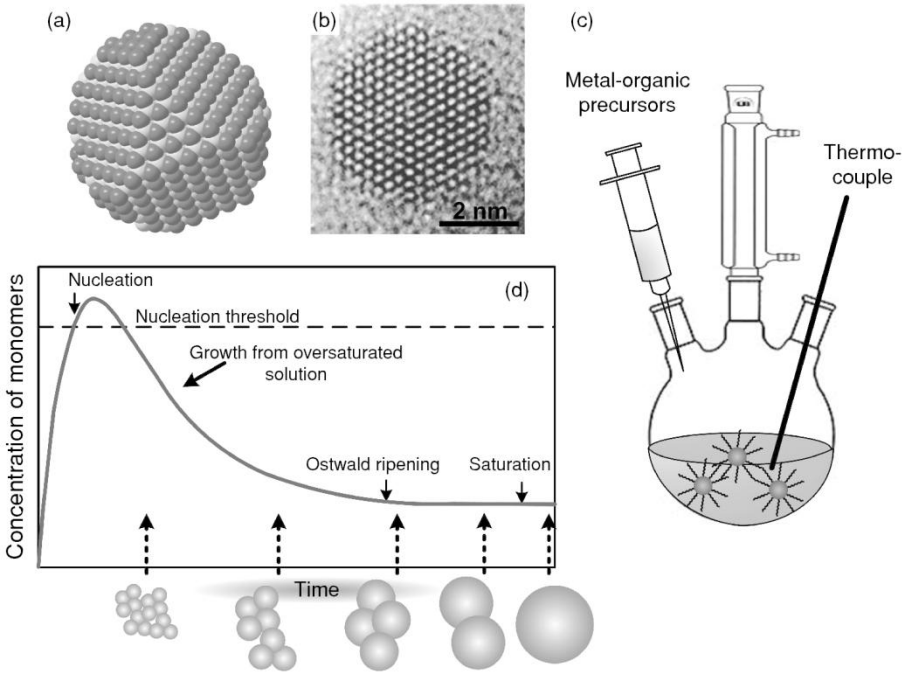

Figure 5. (a) Model and (b) TEM of a single CdSe NC. (c) typical setup used in QD synthesis (d) La Mer model illustration the synthesis of colloidal NCs in relation to concentration of monomers[11,16]

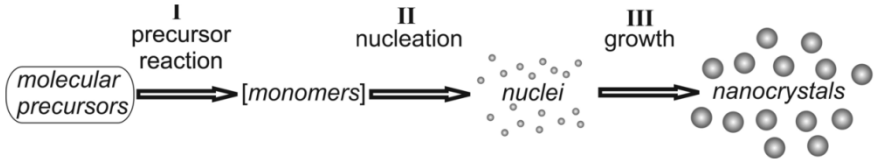

Figure 6. Illustration of the three key steps in the synthesis of colloidal NCs: precursor-to-monomer conversion, homogeneous nucleation, and heterogeneous growth[11]

Film Fabrication Methods

The presence of long-chain surfactant ligands, which are required for the synthesis, colloidal stability, and surface passivation of the QDs, restricts efficient transport of charge carriers over long distances and leads to poor conductivity in films. In order to improve the charge transport, the long-chain surfactant ligands are replaced with short-chain organics or salts through different QD film fabrication methods. This includes solid state exchanges such as spin

coating where a thick QD layer is spin coated on a substrate and soaked in a concentrated solution containing the conductive ligand. A challenge with this method is that the abrupt change from a long-chain surfactant to a shorter ligand between QDs causes film contraction, which can induces cracks, pin-holes, or other defects that can inhibit device performance. Therefore, spin coating QD devices typically require multiple layers of QDs and treatments in order to fill in the cracks in previous layers. Another solid state exchange method is layer by layer dip coating where substrates are dipped into QD solutions and a monolayer or less of QDs are left to dry. The substrate is then dipped into the ligand solution where the ligand exchange occurs. This process is repeated until a desired film thickness is achieved and produces crack free, densely packed, and conformal films. Solution based exchanges involve ligand exchanges in biphasic solutions where the colloidal stability of the exchanged QDs is maintained using high dielectric solvents, that would otherwise aggregate and crash out of solution.[17] Films can then be drop casted, spin coated, or dip coated without inducing cracks or pin-holes seen in solid state exchanges of thick spin coated films. Thermal annealing is also used as a means to remove

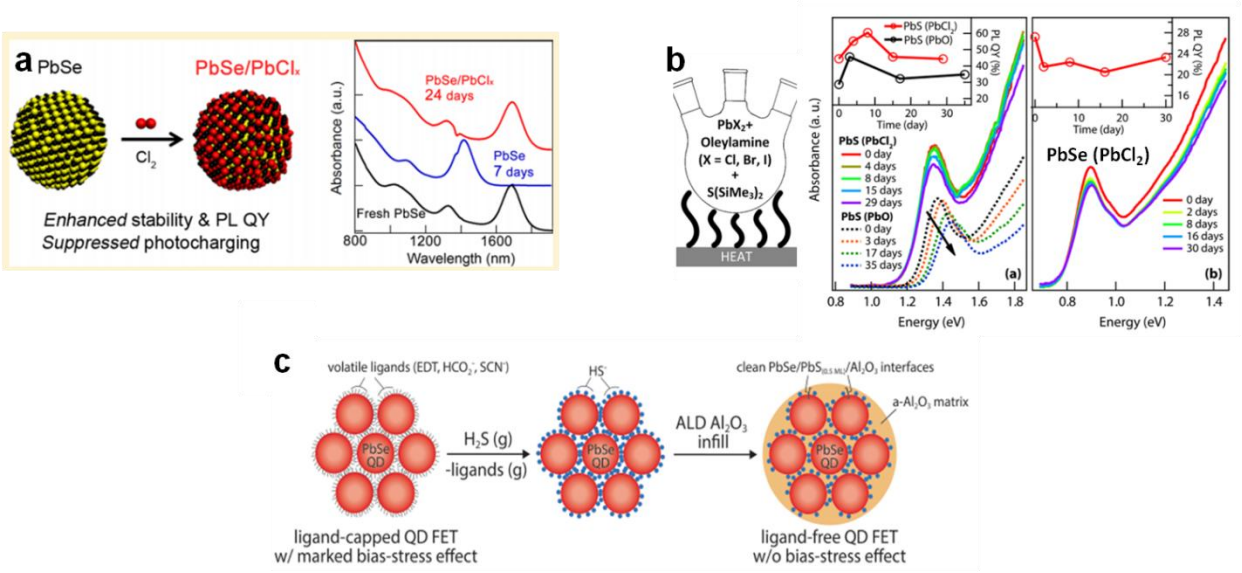

Figure 7. Examples of Passivation Treatments for QD materials. a. Post-synthesis treatments. b.

In-situ passivation utilizing a lead halide as precursor. c. Matrix engineering using alumina ALD infilling

organics. However, the high temperatures used during the annealing to decompose the organics generally sinter the quantum dots and negate quantum confinement effects.

Devices made from ligand exchanged PbX QDs are often characterized by low charge carrier mobilities and small diffusion lengths. This can be attributed to trap states caused by dangling bonds formed during the synthesis or ligand exchange, vacancies, and interfacial defects. [11] In order to understand and improve the performance of PbX QD films, enormous amounts of effort have undergone into studying various passivation treatments and surface chemistries to modify the QD surface (See Figure 7). Synthetic routes utilizing in-situ passivation have been developed to produce PbX QDs with improved performance and air stability. This is done through reacting lead halide salts in oleylamine, which acts as both the coordinating ligand and solvent in the reaction, followed by injecting the anion precursor coordinated to a phosphine or additional oleylamine. The halides, found present on the surface of the QDs, improved the air stability of QDs and enabled devices to be fabricated in air with little reduction in performance.[18] Post-synthetic treatments used in solid state and solution exchanges, as discussed previously, are most commonly utilized for film fabrication. Studied surface chemistries range from assortments of strongly or weakly coordinating, shorter, organic or inorganic ligands such as pyridine[19], hydrazine[20], ammonia[21], thiols[22], thiocyanate[23], halometalates[24], or chalcogenides.[25] The capping of NCs with such ligands enhances electronic coupling between adjacent NCs and allows for the modulation of nearly all practically relevant electronic parameters[26] Low-temperature atomic layer deposition (ALD) has been used to infill

QD films, creating robust, functional QD nanocomposites. It is used to lower the interdot barrier in a quantum dot film to create a more conductive matrix to facilitate charge transport (See Figure 8). The ALD matrix can passivate surface states, decrease the barrier height, and prevent QD oxidation/degradation.[27] The Matt Law Group has demonstrated, in unpublished work, field effect transistor measurements of ALD treated PbSe QD films with record mobilities (μ_n = 14 $cm^2\ V^{-1}\ s^{-1}$), complete air stability, and elimination of bias-stress effect/hysteresis.

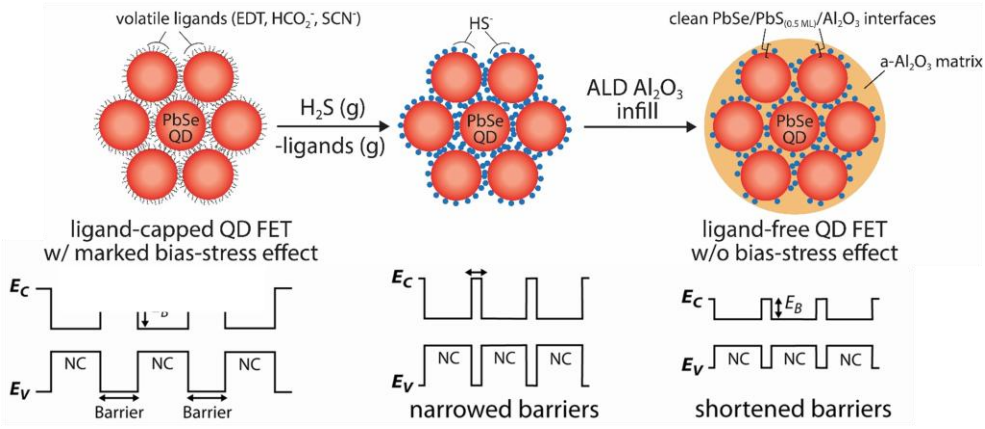

Figure 8. Effect of H_2S and ALD Al_2O_3 infilling on PbSe QDs capped with volatile ligands

Thesis Objective

The focus of this work is to understand the intrinsic nature of PbTe QDs and discover means to study and improve stability of the material. As stated previously, PbTe has a higher dielectric constant, light electron and hole masses that contribute to a larger Bohr exciton radius of 152 nm when compared to PbS (r_{Bohr}= 18 nm) and PbSe (r_{Bohr} =46 nm)[10, 28]. This implies that PbTe QDs can exhibit much stronger degrees of confinement, and lead to greater electronic coupling between neighboring QDs. Increased dielectric screening and reduced number of phonon states, slow hot carrier cooling rates thereby improving MEG efficiency. Despite such promising features, this material has proven difficult to synthesize and fabricate devices. This is owing to its high reactivity and susceptibility to oxidation even in glovebox environments, where surface oxides can easily affect electrical behavior. Unfortunately, the rapid oxidation of PbTe QDs impedes the development of this material and limits available literature resources, in favor of less labile lead chalcogenides, PbSe and PbS. Previous work on PbTe QDs has shown that, in solution, PbTe has the highest MEG efficiency when compared to other lead chalcogenides, as seen in Figure 9[13]. As stated earlier, these measurements were performed on QDs in solution rather than a thin film. Currently, there is only one study of a lead telluride quantum dot solar cell (see Figure 10). While the article reported external quantum efficiencies greater than 100%, the device decayed very rapidly when exposed to air[14]. It is necessary to investigate the stability and the effect of different surface treatments on PbTe QDs in order illuminate possible issues to overcome. To test the electronic characteristics, this study uses field effect transistors as a platform/tool to examine the effect of different surface treatments and relative carrier type in the film.

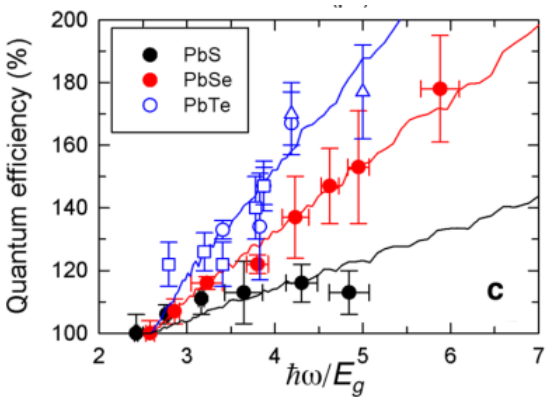

Figure 9. Measured Quantum Efficieny in Solutions of PbS, PbSe, and PbTe QDs[13]

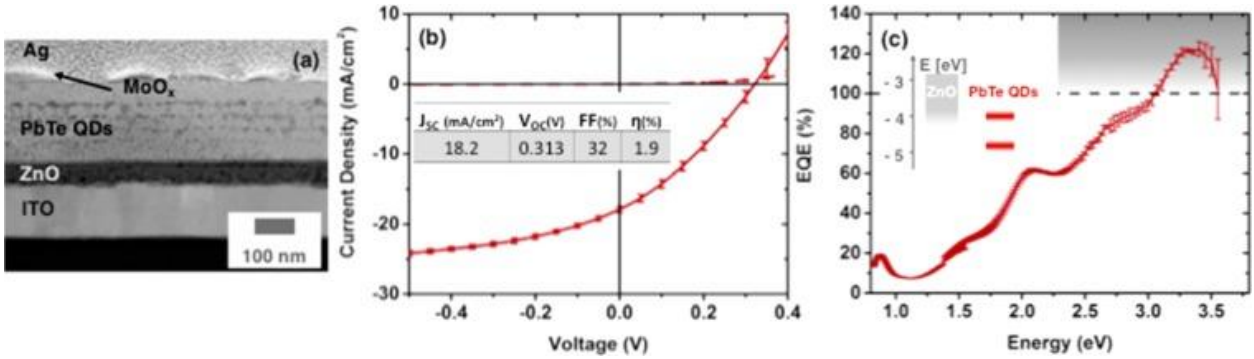

Figure 10. PbTe solar cell displaying (a) cross-sectional image, (b) I-V characteristics, (c) EQE[14]

Chapter 2: Experimental Methods

Quantum Dot Synthesis

As mentioned earlier, quantum dots are typically made by hydrothermal, sol-gel, or solvothermal techniques, the most common of which is the hot injection method. Using this method allows one to achieve excellent control over the desired size of nanocrystals, while maintaining good monodispersity. Simple parameters such as growth time, temperature, and concentration of precursors are used to control the size and polydisperity. By increasing temperature, nanocrystal growth is accelerated, leading to larger sizes. Adjusting the Pb:OA ratio is another pathway to control nanocrystal size. For example, increasing the amount of OA in solution reduces the number of nuclei formed during the injection step due to steric hindrance effects. This allows more monomers to be readily available to diffuse to and react at the QD surface during the growth phase of the nanocrystal, also leading to larger sizes. Below are the precursors and synthesis conditions used to produce the PbTe and PbSe nanocrystals studies in this body of work.

Chemicals: Trioctylphosphine (TOP, 97%) and anhydrous sodium sulfide (Na_2S, >95%) were purchased from Strem Chemical. Lead (II) oxide (PbO, 99.999%), Selenium shot (99.999%) , and Lead Iodide (Ultra dry PbI_2 99.999%) were purchased from Alfa Aesar. Oleic acid (OA, technical grade 90%), Tellurium (99.999% Sigma-Aldrich), 1-Octadecene (ODE,

technical grade 90%), and tetrachloroethylene (TCE, 99%), 1,2-ethanedithiol (EDT, >98%), trimethylaluminum (97%), and anhydrous solvents were purchased from Sigma-Aldrich and used as received.

Synthesis of 3.1 nm PbTe Nanocrystals

The synthesis was performed in a three-neck round bottom flask under air-free conditions using standard schlenk line techniques. The reaction involved Pb:OA ratios of 1:2 and Pb:Te ratios of 1:3. A typical synthesis mixed 3 mmol PbO and 6 mmol oleic acid in 20 mL of 1-Octadecene. At 140℃, 12 mL of 0.75 M TOPTe was injected. After 3 minutes, the reaction vessel was placed in liquid nitrogen and 10 mL of anhydrous hexane was added to assist initial cooling from high temperatures. The vessel was cooled to ~40°C before the round-bottom was removed from the Schlenk line and brought into the glovebox. Subsequent purification was performed in a glovebox with anhydrous reagents. Purification involved three sequences of QD precipitation by ethanol, decanting the supernatant, and re-suspending the QDs in hexanes. All optical characterization was carried out while the dots were dissolved in TCE. Typical yield is roughly 70 mg (5% based on mass of PbO).

Synthesis of 5.5 nm PbTe Nanocrystals:

The Pb:OA ratio was 1:2.6 and the Pb:Te ratio was 1:5. A typical synthesis mixed 6.7 mmol PbO and 17.6 mmol oleic acid in 12.7 mL of 1- Octadecene. At 180℃, 10 mL of 1.5 M TOPTe was injected. After 30 seconds, the reaction vessel was placed in liquid nitrogen and 10 mL of anhydrous hexane was injected to assist cooling and dilute the reactants. The vessel was cooled to ~40°C before the round-bottom was removed from the Schlenk line and brought into the glovebox. Purification followed the same methods as above by performing three washes

using hexane and ethanol as a solvent/nonsolvent pair. Yield was roughly 175 mg (7% based on mass of PbO).

Synthesis of 7.1 nm PbTe Nanocrystals:

The Pb:OA ratio remained1:2.6 and the Pb:Te ratio remained 1:5. A typical synthesis mixed 6.7 mmol PbO and 17.6 mmol oleic acid in 12.7 mL of 1- Octadecene. At 200℃, 10 mL of 1.5 M TOPTe was injected. After 45 seconds, the reaction vessel was placed in a pool of liquid nitrogen and 10 mL of anhydrous hexane was injected. The vessel was cooled until the temperature reached 40℃ and the round-bottom was removed from the Schlenk line and brought into the glovebox. Purification followed the same methods as above by performing three washes using hexane and ethanol as a solvent/nonsolvent pair. Yield is roughly 97 mg (4% based on mass of PbO).

Synthesis of 5 nm PbSe Nanocrystals

The synthesis of medium sized PbSe quantum dots was carried out in an attempt to create the same QD-ligand environment as the PbTe counterparts, to make comparison more reasonable. The Pb:OA mole ratio for PbSe reactions was 1:2.46 and the Pb:Se ratio changed to 1:3.74. A typical synthesis mixed 4.48 mmol PbO and 11.0 mmol oleic acid in 14.0 mL of 1-Octadecene. At 165℃, 8.4 mL of 2 M TOPSe was injected. After 2 minutes, the reaction vessel was placed in a pool of liquid nitrogen and 10 mL of anhydrous hexane was injected to assist cooling and dilute the reactants. The vessel was cooled until the temperature reached 40°C and the round-bottom was removed from the Schlenk line and brought into the glovebox. Purification followed the same methods as above by performing three washes using hexane and ethanol as a solvent/nonsolvent pair. Yield is roughly 25 mg (1% based on mass of PbO).

Fabrication of FETs (Field effect transistors)

The FETs used as a platform for electrical measurements were fabricated in the UCI INRF and BION cleanroom facilities using standard photolithography. The fabrication procedure was developed by Jason Tolentino, as discussed in his dissertation, and is as follows.

Wafers were cleaned in 3:1 H_2SO_4 : H_2O_2 piranha bath for 15 minutes followed by a thorough rinsing with DI water. This step is required to remove organic contaminants. Wafers were dehydrated at 120°C for 15 minutes to drive off any moisture and to prepare the surface for self-assembled monolayer treatment. Vapor deposition of hexamtheyldisilizane (HMDS) in a YES oven to improve adhesion of the photoresist to the oxide wafer. Spin coated Shipley 1827 (S1827) positive photoresist to produce a ~500nm thick polymer film. Spin coat parameters were often adjusted depending on the relative humidity in the cleanroom. Soft bake at 90°C for 10-15 minutes to drive off solvents used in the resist. UV-flood lamp exposure of photoresist coated wafers for 30 seconds using a Chrome photo mask provided by Photo Sciences, Inc. Hard bake at 120°C for 10 minutes. Develop wafers with MF-319 developer at room temperature for 30 seconds and rinse with DI water. Hard bake at 120°C for 10 minutes to drive off excess water and tetramethylammonium hydroxide from the developer. Finally electron-beam evaporation was used to deposit 3 nm of titanium (used as an adhesion layer) followed by 35-40 nm of gold.[30]

QD Film Deposition

A mechanical dip coater mounted inside of a glovebox (DC Multi-4, Nima Technology) was used to prepare PbTe QD films via a layer-by-layer dip coating. The cleaning and deposition processes originated from previous articles published by the Law Group. The substrates (glass, silicon, quartz, or pre-patterned FET) were cleaned by sonication in acetone followed by rinses in acetone and additional sonication in isopropanol and dried under N_2 flow.[27] Substrates were

then soaked for ~15 min in a fresh 100 mM solution of MPTS (mercaptopropyl trimethoxysilane) in dry toluene, rinsed with neat toluene, and dried under N_2 flow. Substrates were mounted on the dip coater arm and deposition began. The process illustrated in Figure 11. For Na_2S treated films, the substrates were alternately dipped into a 2-5 mg/mL solution of QDs in dry hexane and then a 0.05-1 mM solution of sodium sulfide in anhydrous methanol. A third beaker containing neat anhydrous methanol was used to rinse the films after each dip in the sulfide solution in order to remove any residual ions. For EDT treated films, the QD substrates were dipped into 0.05-1mM EDT in anhydrous acetonitrile and dipped into neat anhydrous acetonitrile to rinse. Films were fabricated films with thicknesses in the range of 25−300 nm. Oleate-capped QDs were made by spin coating a 50 mg mL−1 solution of QDs in octane at 600 rpm for 10 s, followed by 1200 rpm for 60 s.[27]

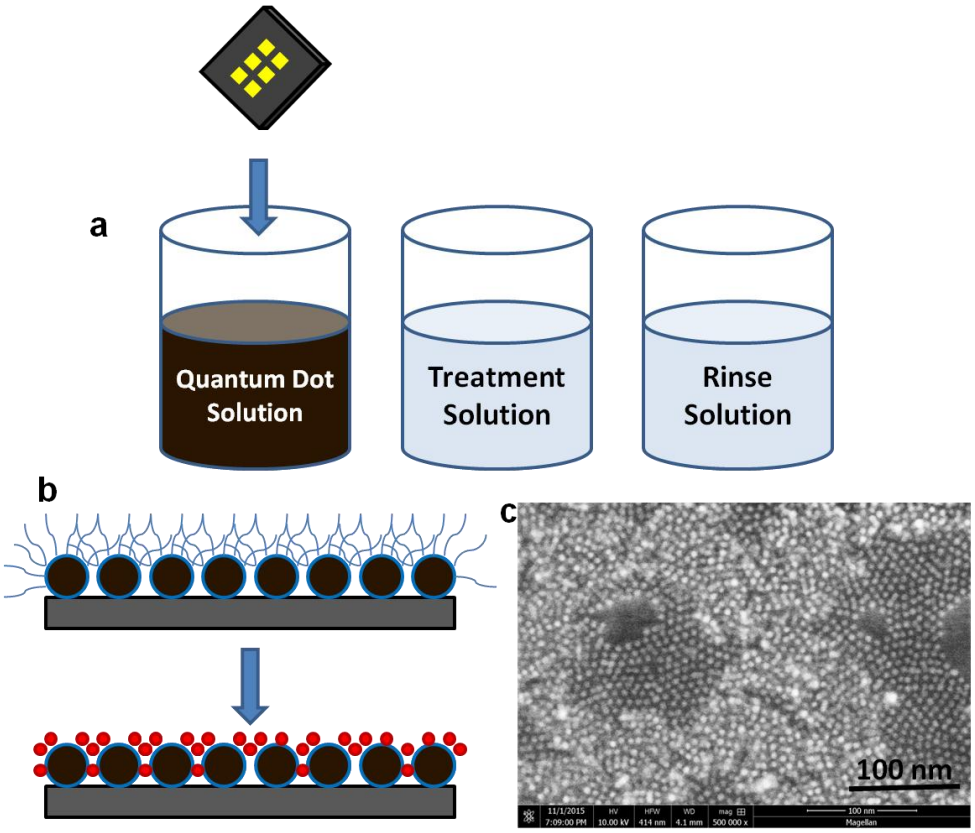

Figure 11. a. Illustration of the layer by layer dip coating process. b. Illustration demonstrating the removal of the oleate through mass action by a higher concentration of the ligand treatment. c. SEM micrograph demonstrating how the dip coating process fills in voids in previous layers creating uniform, densely packed films.

Atomic Layer Deposition Infilling

PbX (X=S, Se, Te) QDs are prone to aggressive oxidation when exposed to air and sintering when presented to elevated temperatures (>100°C). Atomic layer deposition (ALD) has proven successful in preventing oxidative degradation and increasing the photothermal stability of QD films.[31, 32] ALD is a stepwise chemical vapor deposition method for depositing thin conformal films on topologically complicated substrates with submonolayer thickness control.[31, 33] Figure 12a,b demonstrates the ALD process for depositing amorphous alumina. Slow deposition at low temperatures (<80 ˚C) allows for the metal and oxygen precursors to diffuse throughout the interstitial spaces of a QD film without sintering them together. Inhibiting the atomic and molecular diffusion and thereby preventing the QDs from sintering together. ALD can also deposit thick (20-30 nm) overcoats of alumina to serve as a gas diffusion barrier to prevent O_2 diffusion to the QD surfaces. ALD is used to passivate and protect a wide variety of PV materials to reduce surface states and improve electrical behavior. The amorphous Al_2O_3 was deposited in a homemade ALD system within a glovebox from trimethylaluminum and water at a substrate temperature of 54-75 °C and an operating pressure of ~0.1 Torr. TMA pulse and purge times were 20 ms and 60 s, and water were 40 ms and 60 s, respectively.[27,30-33]

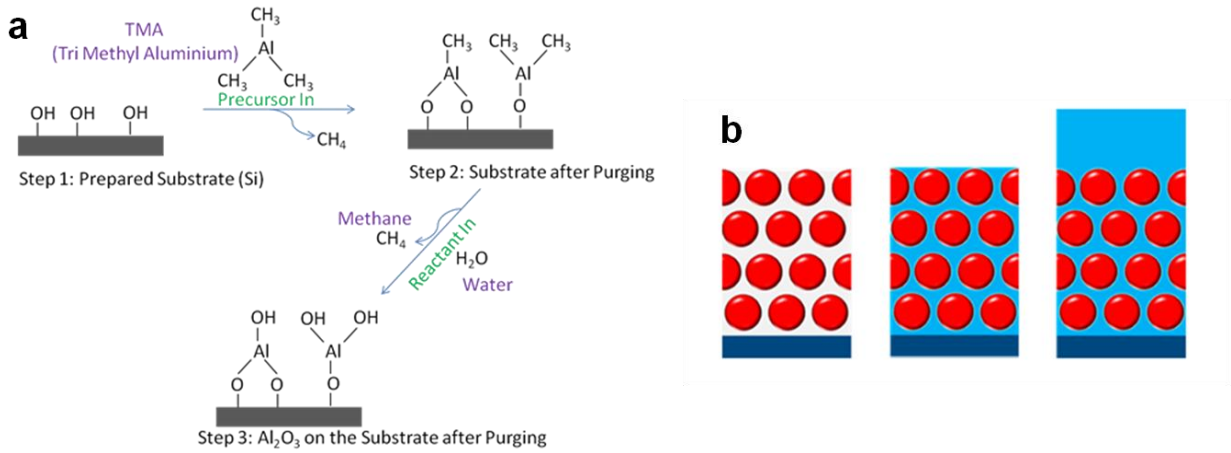

Figure 12 a. ALD process for forming Al-O bonds using TMA and H_2O as precursors. The purge steps ensure the precursors do not react in the gas phase above the substrate. b. Illustion of (from left to right) of an uncoated, infilled and overcoated QD film with alumina (adapted from Ref. 34)

Sample Characterization

Fourier-transform infrared spectra (FTIR) were obtained on a Thermo Scientific Nicolet 6700 spectrometer. UV-Vis absorption spectra were collected using a PerkinElmer Lambda 950 spectrometer. For air-free measurements, an airtight optical cell consisting of two 1.33" mated UHV ConFlat sapphire viewports were used. For general film morphology a FEI Magellan 400 scanning electron microscope was used at 10 kV and 25pA. To determine the size of the quantum dots, a Philips CM-20 transmission microscope operating at 200 kV was used. Transistor measurements at room temperature were performed in a nitrogen filled glovebox with a probe station using a Keithley 2636A dual-channel SourceMeter and Keithley 238 SourceMeter (for gated 4-point transistor measurements) driven by homemade LabView software. X-ray photoemission spectra (XPS) were acquired on a Kratos Axis Supra photoelectron spectrometer at a base pressure of 10^{-9} mbar. X-ray spectra were acquired using monochromatic Al Kα radiation. Facility calibration was performed by measuring Fermi level

energy of a sputter-cleaned Ag. High-resolution elements peak spectra were collected at 20 eV pass energies using a 0.1 eV step size, 300 ms dwell time and 2-5 sweeps per spectrum.

Field-Effect Transistor Measurements

QD films were dip coated onto degenerately doped silicon substrates coated with a 200 nm thick thermal SiO_2 gate oxide and pre-patterned with source/drain electrodes (3 nm Ti/35 nm Au, 25 μm channel length, 1000 μm width unless otherwise noted). QD film thicknesses of ~40 nm were used (See Figure 13a). The perimeter, edges, and backside of each QD film was wiped clean with a swab to eliminate parasitic gate currents and provide a clean spot for contacting the gate electrode. The substrate was mounted on the probe station in a N_2 filled glovebox and measurements were performed. Applying a source-drain (SD) and gate voltage across the channel offers the capacity to extract information such as electron and hole field effect mobility, majority carrier type, current transient decay rate and current hysteresis. Output curves are generated by holding the gate voltage constant and sweeping the SD bias. As the SD voltage increases, the current also increases linearly until the QD film becomes saturated and is unable to pass larger amounts of current. Transfer curves do the opposite by sweeping the gate voltage while keeping the SD bias constant, as shown in Figure 13b in the ideal case.[31] When QD films have high carrier concentrations or trap states, the gate voltage will have little impact and poorly modulate the film as shown in Figure 12b in the non-ideal case. Linear mobilities, μ_{lin}, were calculated from transfer curves acquired at $V_{SD} = \pm 10$ V (with positive V_{SD} for electrons and negative V_{SD} for holes), according to the gradual channel approximation equation in the linear regime:

$$\left.\frac{dI_D}{dV_G}\right|_{V_{SD}=\text{constant}} = \frac{WC_{ox}V_{SD}}{L}\mu_{lin}(V_G, V_{SD})$$

where the channel width is W, the channel length is L, and the capacitance of the gate oxide per unit area is C_{ox} (17.5 nF cm^{-2}). The slope of the transfer curves for linear mobility calculations was measured at V_G = ±40 V such that the current consists of primarily electrons or holes.

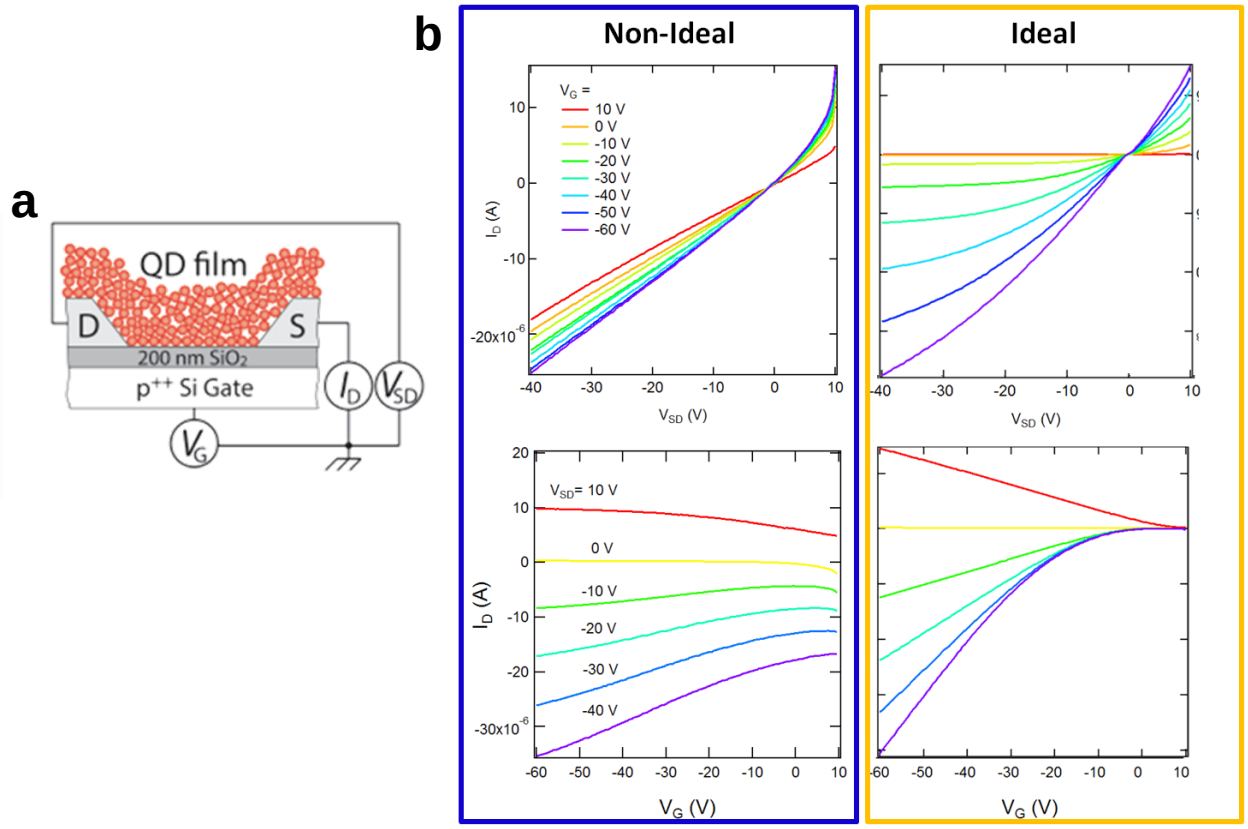

Figure 13 a. Illustration of bottom contact FET. b. (left) Example of a non-ideal FET with poor gate modulation. (right) Example of an ideal p-channel FET with good modulation.

Chapter 3: Structural, Optical and Electrical Properties of PbTe QDs

Monodisperse PbTe QD Synthesis

At the beginning of the study, it was necessary to determine conditions to develop different sizes of the PbTe nanocrystals. Due to quantum confinement, the optical and electronic properties of quantum dots change with size and it is necessary for future studies to have synthetic conditions set in place. This was done by adjusting concentration of the precursors, growth time, and temperature as explained in earlier sections. Three nanocrystal sizes were successfully synthesized. From TEM analysis, the average diameters were 3.6 , 5.2 and 7.7 nm and had a first excitonic absorption peak at 1270, 1445, and 1890 nm, respectively, as shown in Figure 14. The samples were relatively monodisperse with all sizes showing cuboctahedron particles. A majority of the data presented here will be utilizing ~5 nm PbTe QDs from different nanocrystal batches, as each reaction produced low yields of NCs.

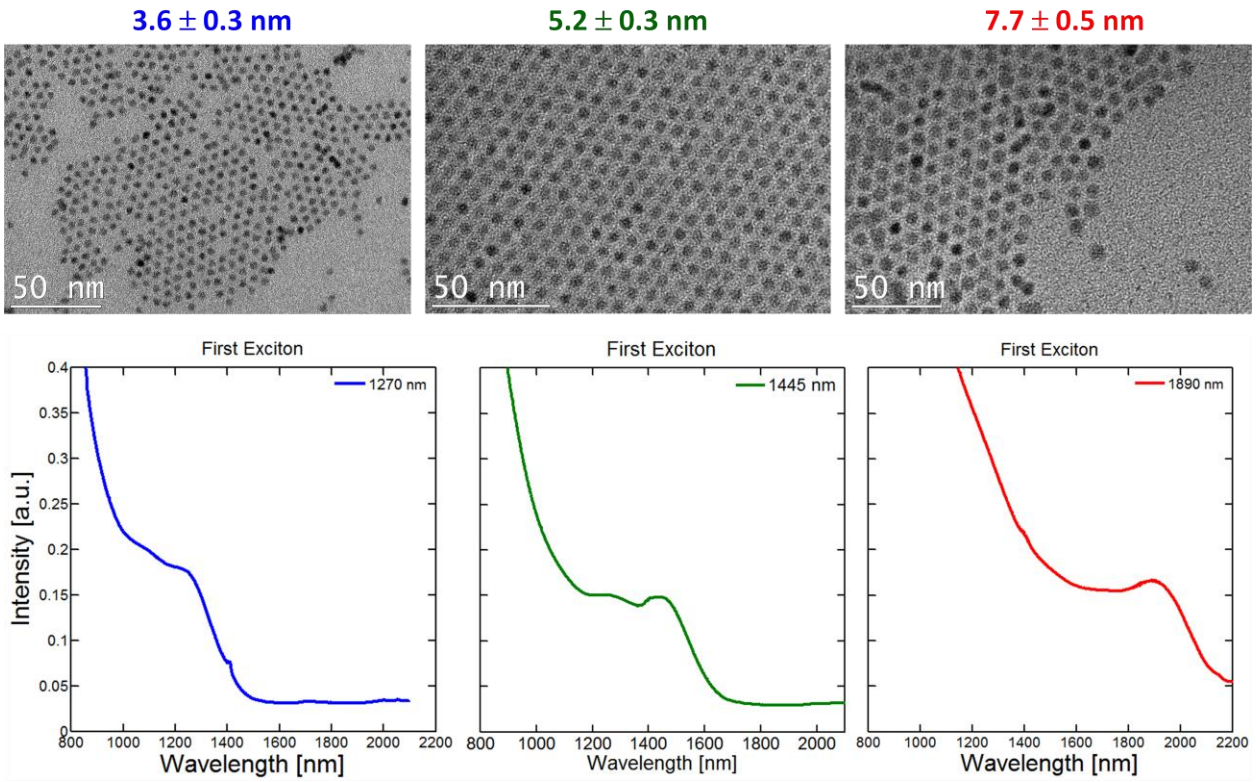

Figure 14. TEM micrographs and absorption spectra of PbTe nanocrystals of sizes 3.6 ± 0.3, 5.2 ± 0.3 and 7.7 ± 0.5 nm

Stability of PbTe QDs

Figure 15 shows the results of air exposure of an oleate capped PbTe QD solution in TCE (tetrachloroethylene) and a thin film. In the solution spectra, after air exposure, the first exciton shifted to higher energies and its absorbance rapidly decreased. It took about 150 min for the definition from the first exciton peak to completely wash out. In the thin film, this effect was seen five times faster than in solution and the first exciton was no long distinct after a mere 30 min. This suggests that the PbTe QDs are oxidizing in a non-uniform fashion. As the dots are oxidized, the PbTe are converted into different oxide species that form a shell that becomes

thicker over time and reduces the effective size of the PbTe nanocrystal. This would cause blue shifting and broadening of the first excitonic peak, as smaller dots have larger band gaps and as they oxidize non-uniformly, the size distribution increases. The difference in the oxidation rate between the solution and thin film is due to the increased time it takes for oxygen to diffuse into the solution versus a film where the dot surfaces are directly exposed to air.

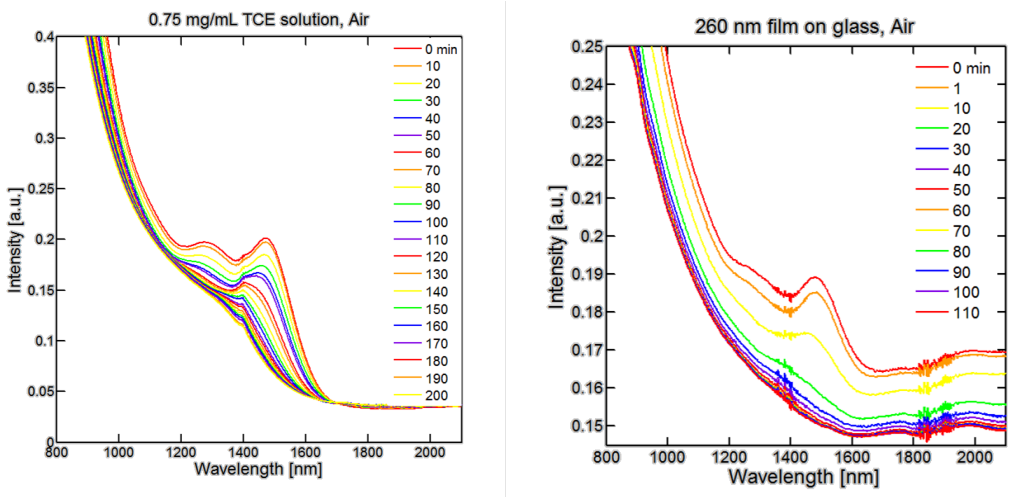

Figure 15. Absorption spectra of air exposed ~5 nm oleate capped PbTe QDs in TCE solution (Left) and in a 260 nm film on glass (Right)

When PbTe QDs are in a nitrogen environment such as a glovebox, their stability is drastically improved when compared to ones exposed to air as shown in Figure 16. The nitrogen exposed PbTe QDs stored in TCE slowly change over time, with small amounts of blue shifting, indicating a decrease in size, or etching. This can be attributed to small amounts of oxidation over time within the glovebox or a possible etching effect from the solvent.

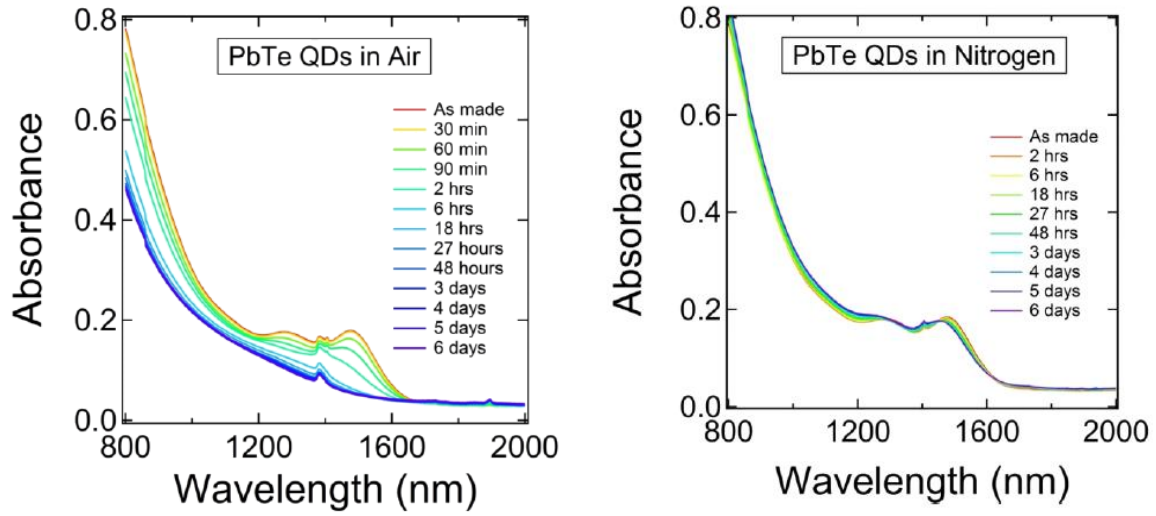

Figure 16. Absorption spectra of air exposed (left) and nitrogen environment exposed (right) ~5 nm PbTe QDs in TCE solution. *Data collected from former undergraduate, Glen Junor

To show the drastic effect of oxygen on PbTe QDs, oleate capped PbSe QDs of the same shape and size are used to compare stability as it is less labile. Figure 17 shows the expected result for oxidation of PbSe. There was no noticeable blue-shifting until 48 hours of air exposure and no significant peak broadening as compared to PbTe samples.

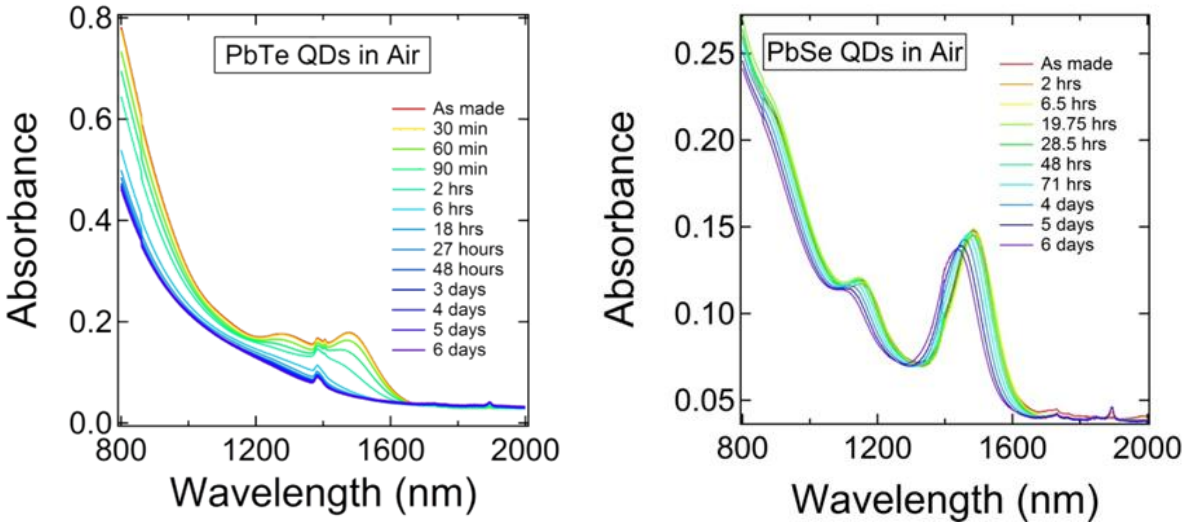

Figure 17. Absorption spectra of air exposed oleate capped PbTe QDs in TCE (Left) and PbSe QDs in TCE (Right) *Data collected from former undergraduate, Glen Junor

The effect of oxidation in PbTe QD films is accelerated when the film undergoes ligand exchange. Figure 18 shows a PbTe film treated with EDT (1,2-ethanedithiol). Within the first minute of air exposure the first exciton drastically washes out and within 10 minutes is nearly completely gone. The increase in oxidation is due to the loss of the oleate shell that formerly covered the QD surface. The long chain oleate ligand not only acts as an electronically insulating shell, but it also provides a physical barrier, to a certain degree, to air. The EDT ligand while electronically conductive, is much shorter and enables air to more easily diffuse to the quantum dot surface and oxidize it.

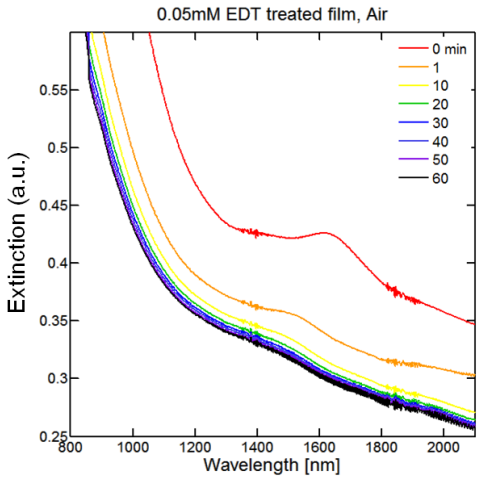

Figure 18. UV-Vis spectra of PbTe-EDT thin film exposed to air

XPS was utilized as another method to examine oxidation of PbTe films treted with EDT. All samples were transported air-free into the analyzing chamber and measured. All XPS measurements were performed by Chao Yi. The samples were then taken out and exposed to air for 5-10 min durations, after which, they were placed under vacuum and measured again. Data

was collected and presented in Figure 19. Before air exposure, only the Pb^{2+} and Te^{2-} peaks are present (Figure 19a, b). This is to be expected for a freshly fabricated PbTe sample that has not been exposed to air. There is also evidence of sulfur in the film due to the EDT treatment (Figure 19c,d). Lastly, there is no presence of oxygen in the film as indicated in Figure 19e by the lack of

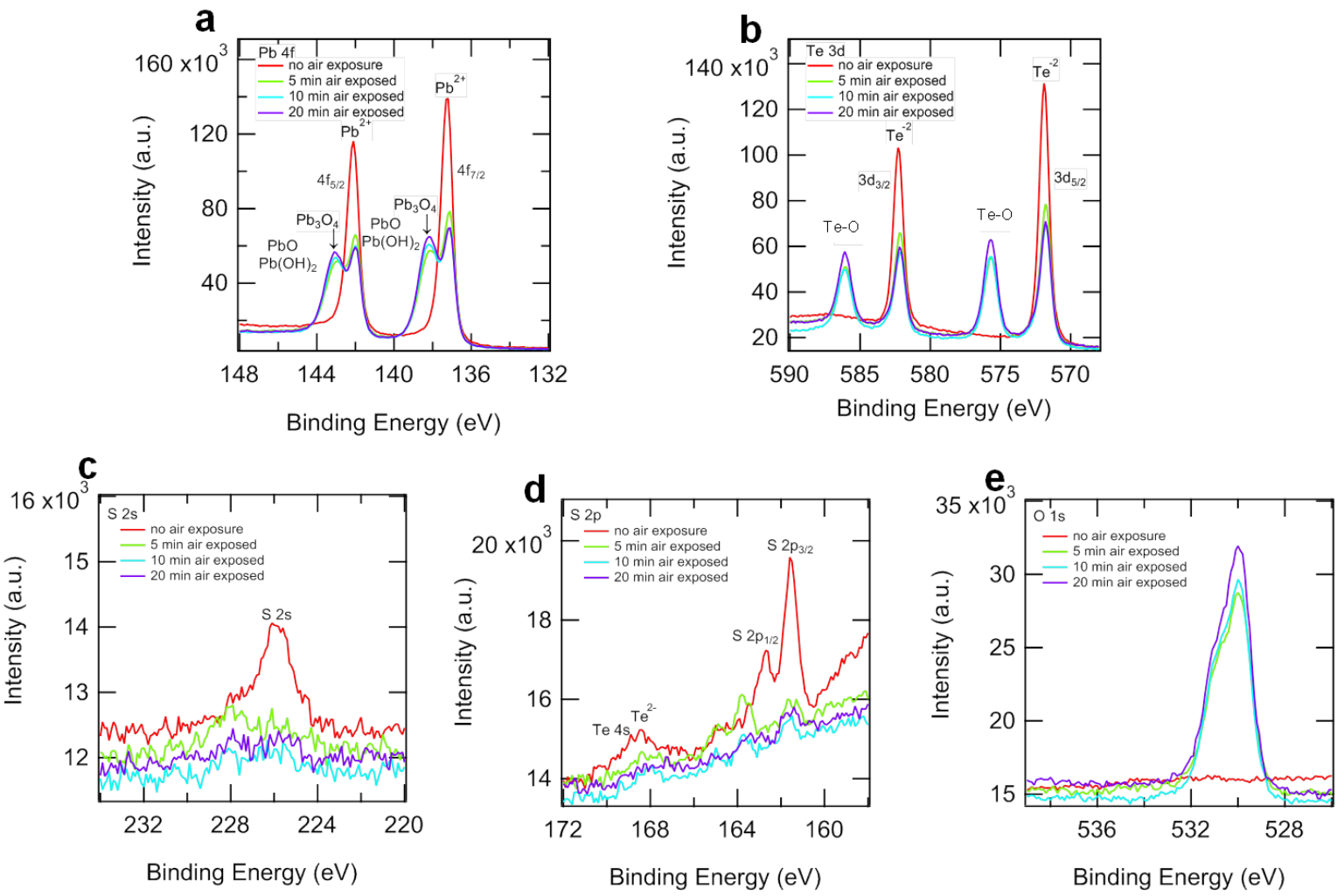

Figure 19. XPS spectra of an EDT treated PbTe QD thin film oxidized over time. Scans were taken at a. Pb 4f, b. Te 3d, c. S 2s, d. S 2p, and e. O 1s regions.

a peak in the O 1s region. After air exposure, Pb and Te spectra both show the presence of oxygen bonds as signified by the additional peaks. The intensity of the Pb^{2+} and Te^{2-} peaks also

diminish as the PbTe is converted to oxides. The presence of the sulfur within the film is now gone as the EDT exposed to air becomes volatile and is removed from the QD surface. Lastly, the appearance of a broad oxygen peak in Figure 19e becomes apparent after air exposure. The broad peak is most likely due to a convolution of the different oxides that have formed within the film. After more air exposure, the intensities of the Pb^{2+} and Te^{2-} peaks continue to decrease, although not as dramatic as the initial air exposure, whereas the Pb-O, Te-O, and O peak intensities increase. At this time, an oxide shell has most likely formed and could be slowing the diffusion of oxygen into the remaining pristine QD film.

The atomic ratios were determined using the relative peak areas and dot size used in the air free sample. The ratio of Pb:Te was found to be 1.31:1. This indicated that the surface of the film is Pb rich which is consistent with literature data that obtain a Pb: X ratio of 1.25-1.5.[29] This should indicate that the film has n-channel behavior when the electronic properties are measured on a FET. However, as will be discussed in the next sections, the films are found to have strong p-channel behavior. This discrepancy could be due to surface oxides that are already on the film whose concentrations are below the detection limit of the XPS, but contribute greatly to the electronic properties of the film.

Thiol Treated PbTe QDs

Na_2S Treated Films

Oxidation, optical and electronic effects are much more pronounced in QD materials after the long chain surfactant is replaced with a much shorter, conductive ligand. This removes the large electronically insulating barrier and the interdot distance decreases thereby improving electronic coupling between quantum dots. Figure 20 shows the optical and structural changes that occur after the ligand exchange process. After ligand exchange, the absorption spectra for

both materials demonstrated significant red-shifting and broadening in the first exciton peaks. The red-shifting occurs due to the change in the dielectric environment surrounding the QDs, since they are now surrounded by conductive salts rather than insulating ligands. The broadening features are mainly due to the improved coupling between dots since the interdot distance has been drastically reduced. It is also possible that the dots may have necked together creating effectively a larger size distribution. The TEM images of the exchanged dots agree with the absorption spectra since there are dots necked together. Figure 21 shows the percent of ligand exchange or the amount of oleate still left on the surface of the nanocrystal. The films are all the same thickness and same dot size and can be used to quantify the exchange by comparing the integrated area under the C-H stretching region at ~3000 cm^{-1} with the oleate treated and sodium sulfide treated films. Both films had an exchange rate >95% which means nearly all of the oleate has been removed. The residual C-H stretching could be due to oleate or solvent that may have not evaporated completely from the film during the dip coating process.

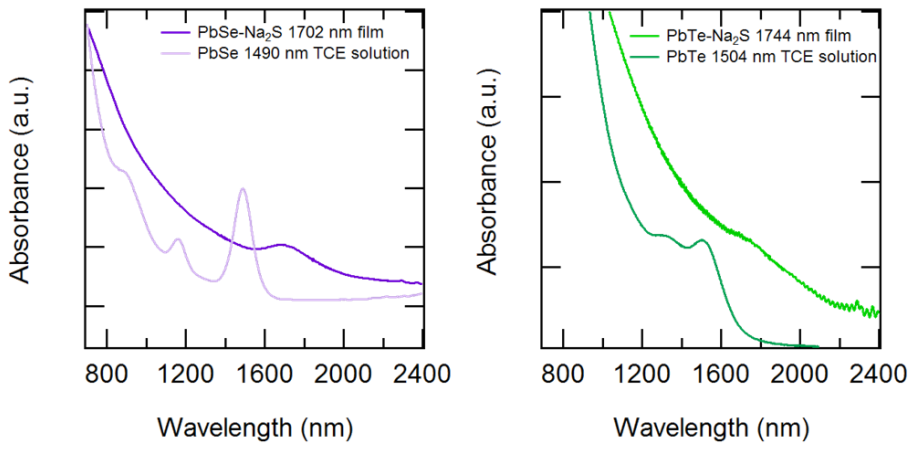

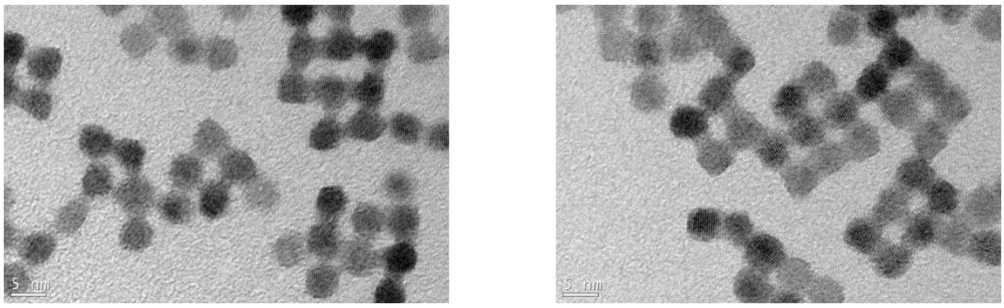

Figure 20 Absorption spectra of ~5 nm Na_2S treated PbSe (top left) and PbTe (top right) QDs. TEM micrograph of Na_2S treated PbSe (bottom left) and PbTe (bottom right)

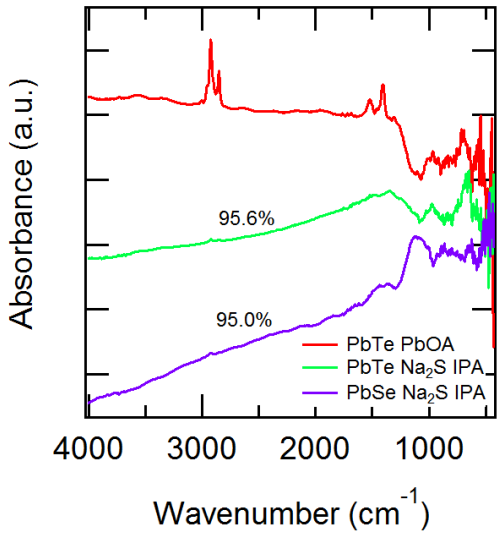

Figure 21. FTIR spectra of ~40 nm oleate capped PbTe and ~40 nm Na_2S treated PbSe and PbTe QDs

In order to make effective comparisons between PbSe and PbTe, it is necessary to try and minimize possible problems. One of which is the morphology of the treated PbTe films when compared to PbSe. As shown in Figure 22, the treated PbSe film is uniform and densely packed with nanocrystals. Upon examining the treated PbTe film, it was found that the quantum dots necked together in a fashion that created a porous film. A porous morphology can degrade device

performance as it will hinder charge transport through the film and create pin-holes or other defects that can act as recombination centers in photovoltaics. Different approaches were made to improve the morphology of the treated PbTe films. They include changing the rate at which the substrate entered and left the quantum dot solution, soaking for longer times at lower concentrations, altering solvents, and adjusting quantum dot concentration. As shown in Figure 23, increasing the quantum dot concentration to 5 mg/mL made the some improvements, but the film was still porous and the dots were still aggressively necked.

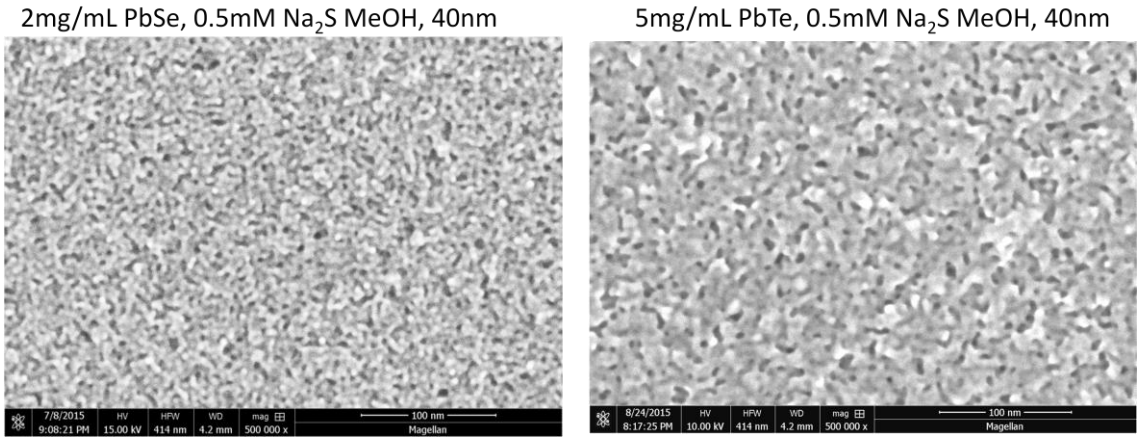

Figure 22. Na_2S treated PbSe (left) and PbTe (right) displaying different film porosities

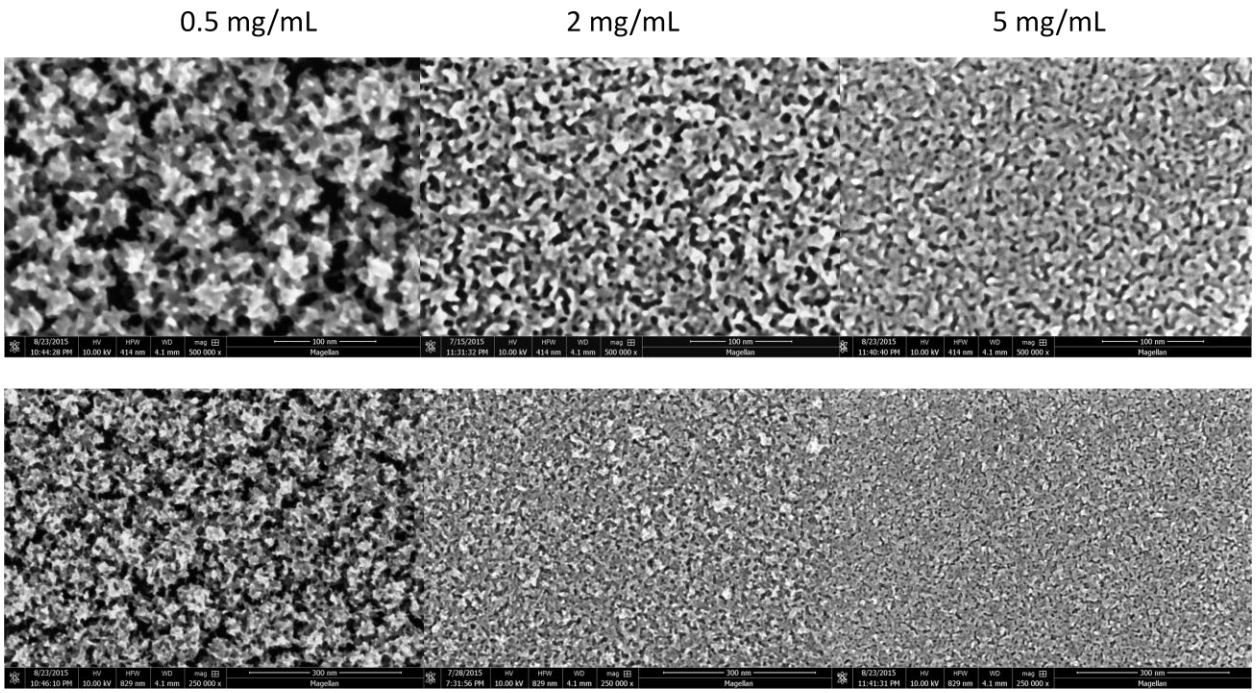

Figure 23. QD concentrations used during the dip coating process. 0.5 mg/mL (left column), 2 mg/mL (middle column), 5 mg/mL (right column)

EDT Treated Films

Due to the porosity in the Na_2S treated films, alternative ligands were explored. EDT treated films were found to form uniform, densely packed films as shown in Figure 24. They also achieved complete ligand exchange as shown in the FTIR spectra of Figure 25, where the residual C-H stretching is due to the EDT ligand itself. When examining a single monolayer, the TEM images of the EDT treated dots (Figure 26) were not as fused as the Na_2S treated ones, owing to the longer length of the EDT molecule. However, as will be shown in the next section the electronic properties of EDT treated PbTe QDs vary from PbSe.

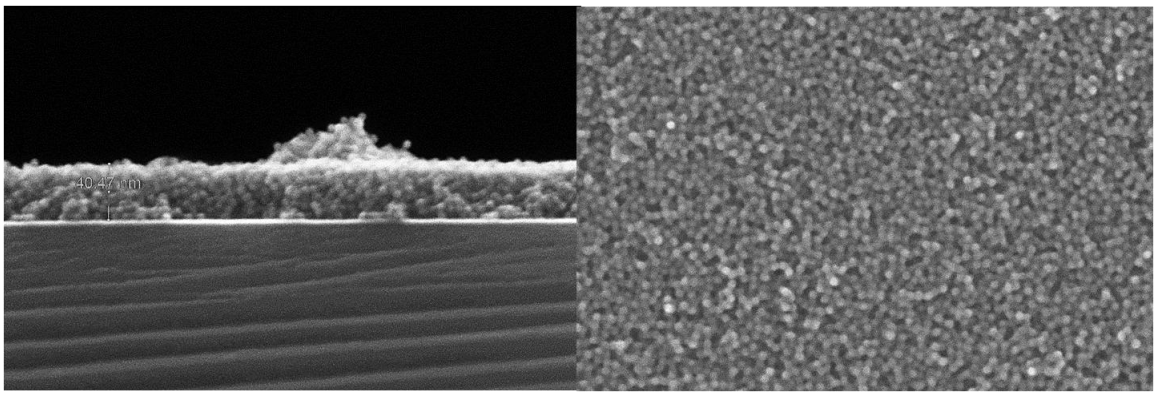

Figure 24. SEM micrographs of EDT treated PbTe QD film. (left) cross sectional image. (right) top-down image

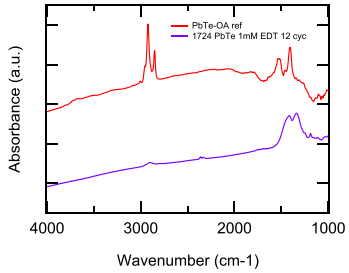

Figure 25. FTIR spectra of ~40 nm of oleate capped PbTe (red) and EDT treated PbTe (purple)

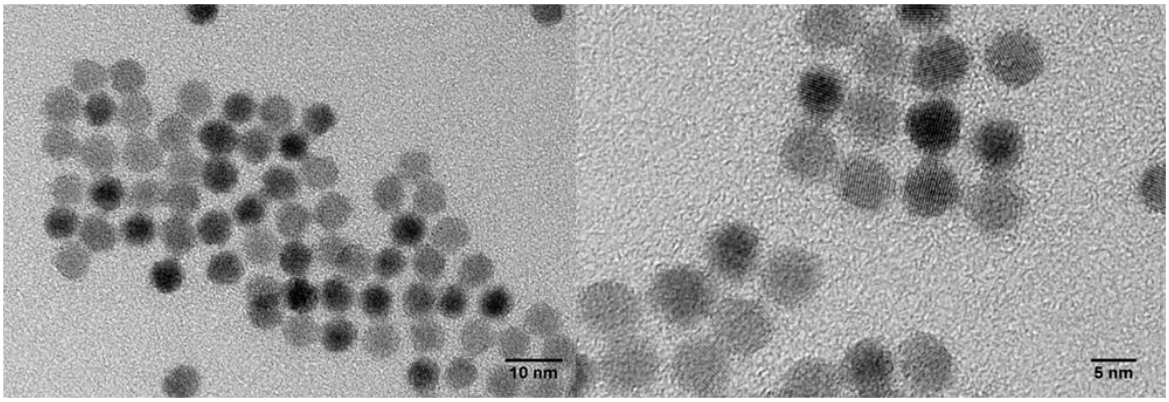

Figure 26. TEM micrographs of EDT treated PbTe monolayers

FET characteristics

To begin to evaluate a semiconductor for a possible photodiode, FETs are used as tools to characterize the electronic properties of the material. Figure 27 shows the transfer, output, and transient characteristics of Na_2S PbTe and PbSe films. Both samples show that holes are the majority carrier type. This is determined based on the slope of the transfer I-V curve and applying the gradual channel approximation to determine mobility. It is also evident that both films have large charge carrier densities since the output curves show little gate modulation. Lastly, the transient curves show current is maintained over time and are used to indicate possible trap states or thermally activated bias stress effects in the material. In both films, the transient is very poor, so it is necessary to either passivate the trap states in some manner or cool the films down to liquid nitrogen temperatures to eliminate thermally activated motion and reduce the carrier concentration in the films so that they can be modulated by the applied gate.

EDT treated devices exhibit better gate modulation when compared to Na_2S treatments. As shown in Figure 28, the applied gate voltage can modulate the PbTe film much better, but the overall behavior is still not ideal for FET devices. The PbSe FET device behaves quite well and exhibits ambipolar behavior since the film can conduct both electrons and holes with decent mobilities.

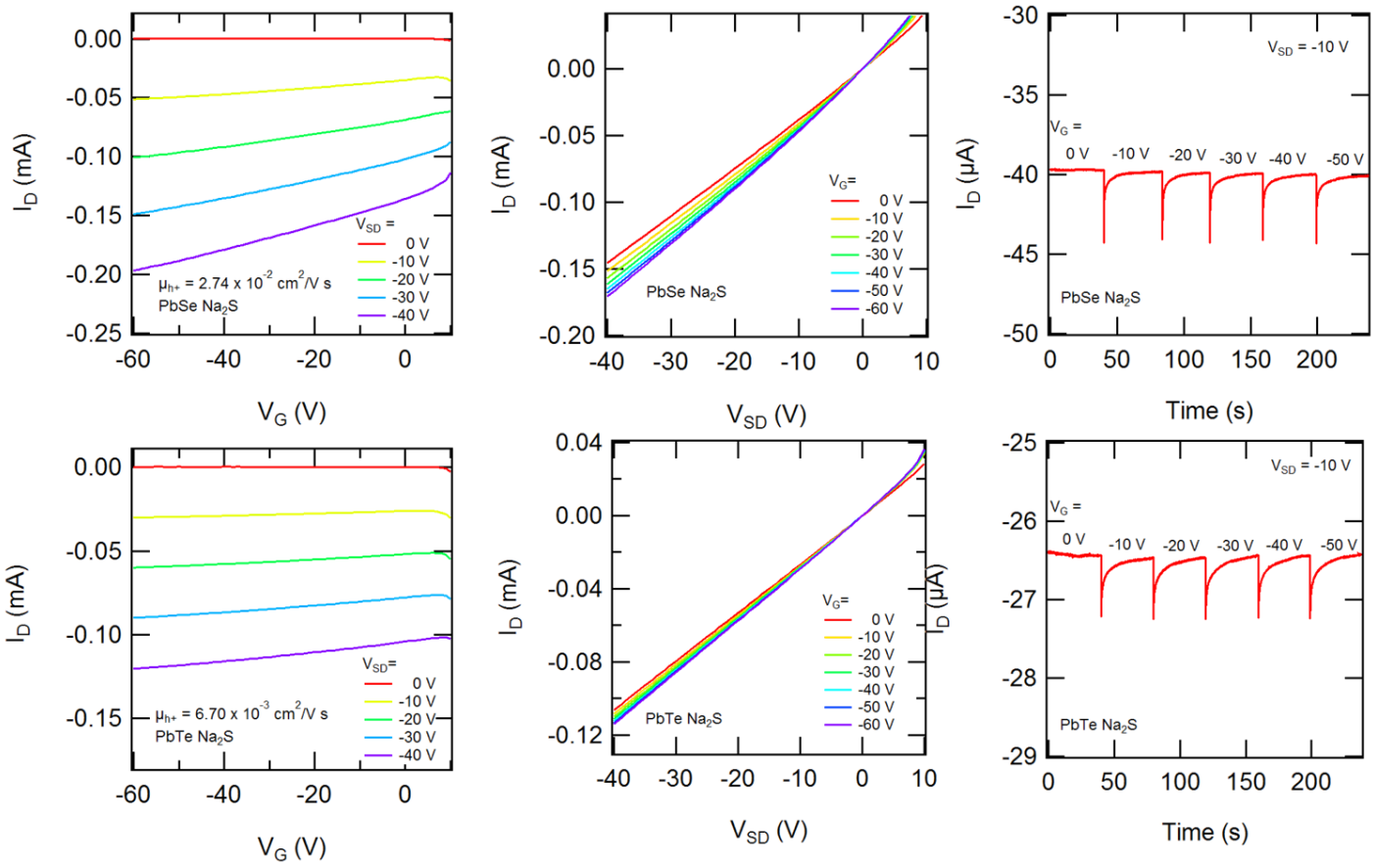

Figure 27. FET I-V plots of Na_2S treated PbSe and PbTe films. PbSe transfer plot (top left), PbSe output plot (top middle), PbSe transient measurement (top right). PbTe transfer plot (bottom left), PbTe output plot (bottom middle), PbTe transient measurement (top right).

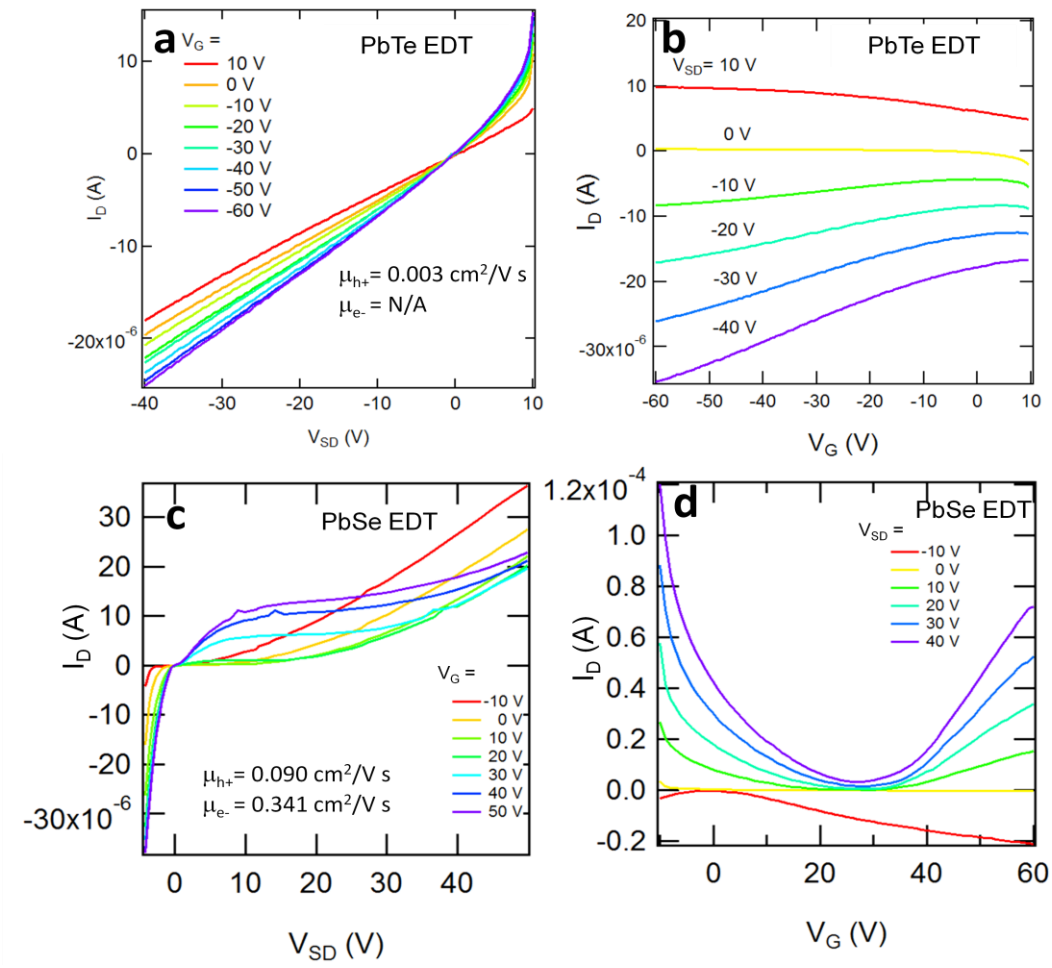

Figure 28. FET I-V plots of EDT treated PbSe and PbTe films. PbTe transfer plot (top left), PbTe output plot (top right), PbSe transfer plot (bottom left), PbSe output plot (bottom right),

Effect of Alumina ALD Treatment

Using Atomic Layer Deposition (ALD) is one method as discussed earlier to passivate trap states and can dope the film. Figure 29 shows a Na_2S treated PbTe FET infilled with ~20 nm of alumina. Before the ALD process, the film has a low hole mobility, poor gate modulation, and bad transient behavior. After the ALD process, the film has changed to n-channel behavior or electrons as the majority carrier within the film. The film can now be modulated effectively by

the gate, the transient characteristics have improved, and the electron mobility has drastically increased to around 1.8 cm^2/Vs.

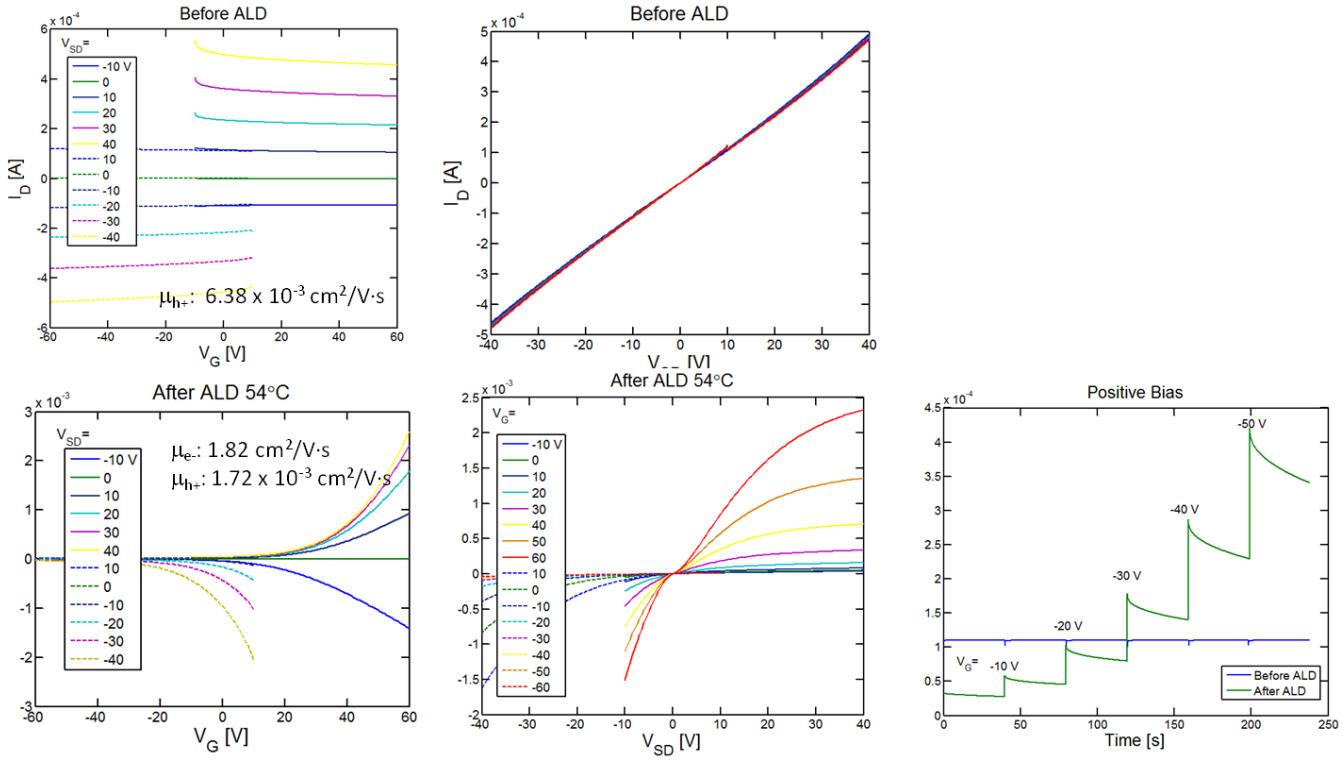

Figure 29. PbTe-Na_2S FET characteristics. (Top Row) Transfer and output characteristics before ALD. (Bottom row) Transfer, output and transients characteristics after ALD

The application of ALD also greatly improves the stability of QD films by creating a barrier against gas diffusion, preventing oxidation, and diffusion between QDs that can lead to loss of quantum confinement. This is evident in Figure 30 where a PbTe film is treated with EDT and alumina ALD. The films with and without ALD are exposed to air. As expressed earlier, the film with no ALD treatment oxidizes with a rapid loss of the first exciton peak. The alumina treated film does not show any signs of aging or degradation in air and has remained so for three

months. Similar effects can also be seen in the FET characteristics, as shown in Figure 31, the EDT treated film changed from p-channel to n-channel behavior after ALD treatment with an electron mobility of 0.66 cm^2/Vs. The FET characteristics, including the electron and hole mobilities, also remained stable after about one month of air exposure (see Figure 32).

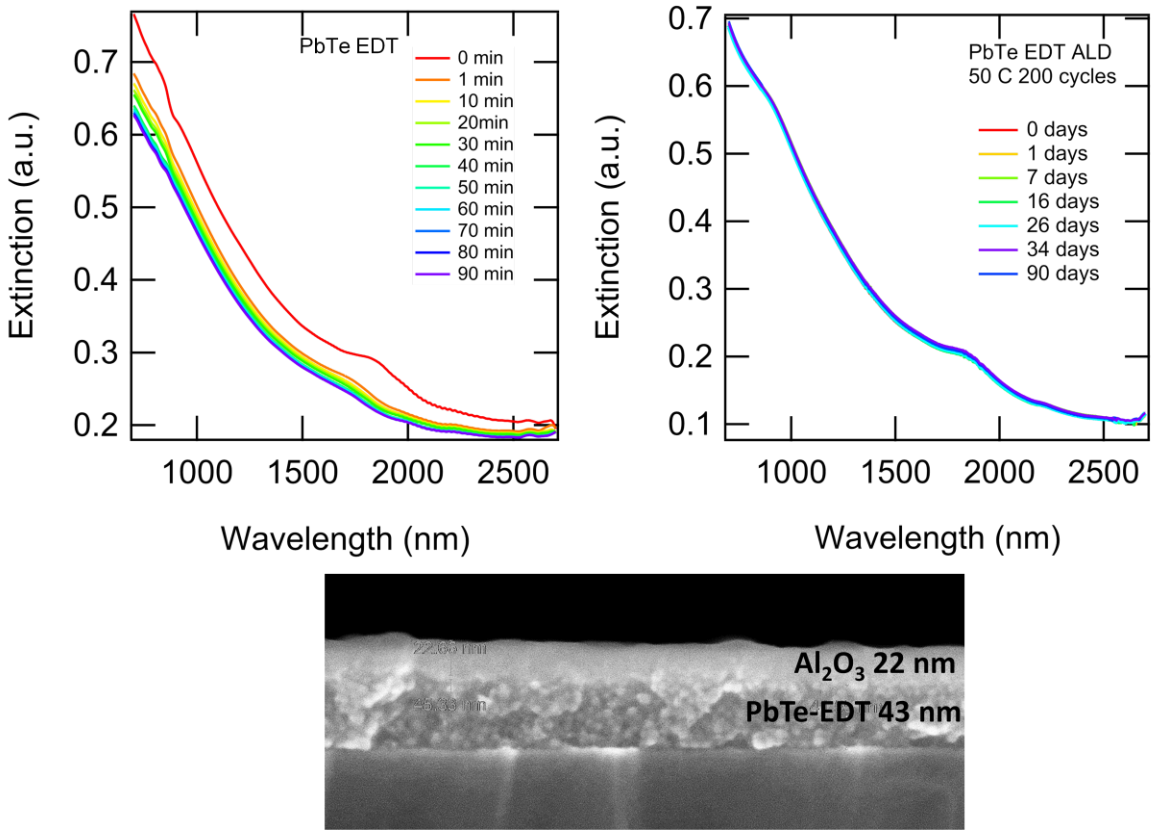

Figure 30. Absorption spectra of PbTe-EDT films (Left) with no ald treatment, and (Right) with ald treatment. (Bottom) SEM micrograph of ALD treated PbTe-EDT film

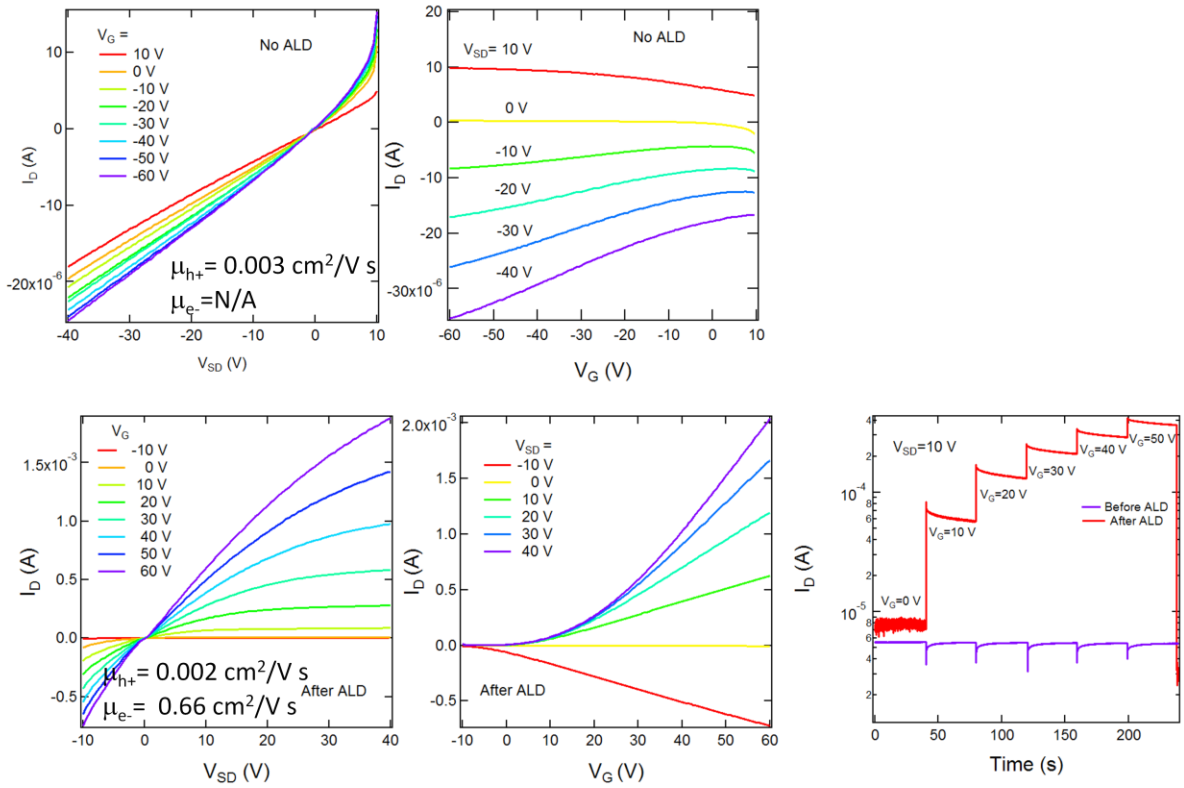

Figure 31. FET measurements of PbTe-EDT films. (Top Row) Transfer and output characteristics before ALD. (Bottom row) Transfer, output and transients characteristics after ALD

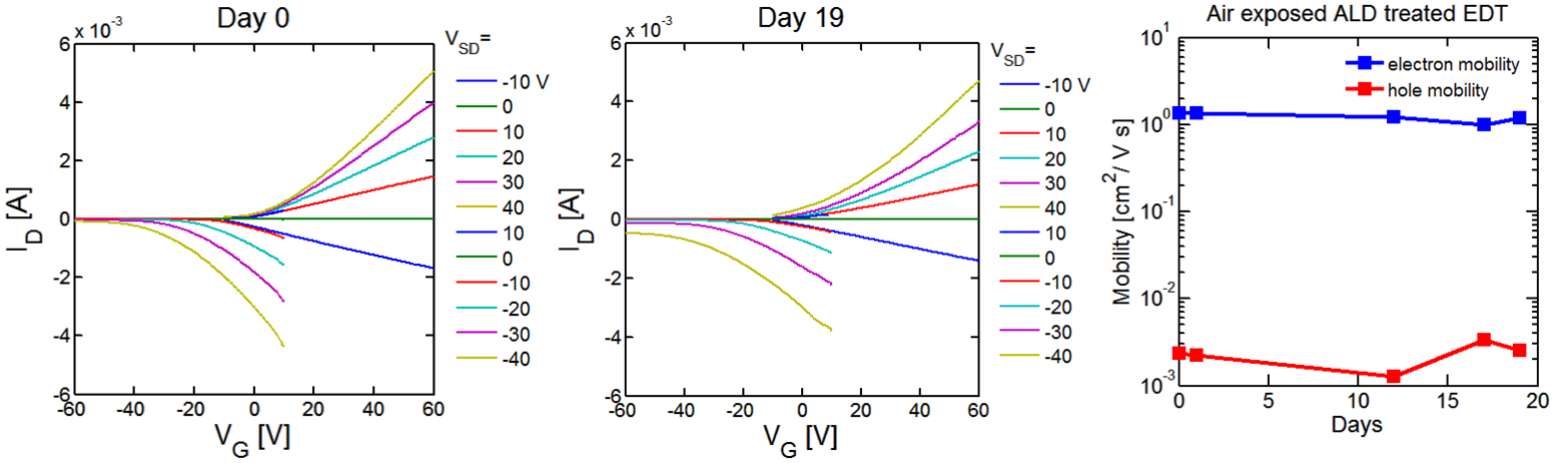

Figure 32. Air Exposed ALD treated PbTe EDT FET. (Left) Transfer characteristics at day 0. (Middle) Transfer characteristics at day 19. (Right) Measured electron and hole mobility. *Note FET was damaged after Day 19 and could no longer be used to acquire data

Chapter 4 Synthesizing Large PbSe QDs for SWIR Photodetectors

Short-wavelength infrared (SWIR) cameras and photodetectors have already been shown to produce clear images and good sensors under unilluminated outdoor conditions. These existing infrared imaging technologies are very expensive because it involves epitaxial growth of compound semiconductors (InGaAs). Solution processed materials have the potential to bring tremendous improvements to security systems and consumers electronics applications due to reduced cost, ease of scale up, and tunable optical absorptions, in the case of quantum dots. PbSe quantum dots are good materials for this application since they have small band gaps and can easily absorb light in the IR region. The goal was thus to develop a PbSe photodector with absorption wavelengths at ~2500 nm with record detectivity. The participation in this project, as demonstrated in this thesis, was to synthesize the large PbSe QD. The construction and testing of actual devices was performed by Chao Yi.

Synthesis of Large PbSe QD (~2500 nm)

As stated in earlier sections about synthesis, the size of the nanocrystal can be easily adjusted using parameters such as concentration of precursors, temperature, and growth time. All

of which were used to increase the size of the nanocrystals. As shown below in Figure 33, high temperatures and growth times were necessary for some size improvements. But adjusting the Pb:OA ratio had the greatest impact to achieve the ~2500 nm absorption. This is accomplished by reducing the number of nuclei and enabling more monomer available to diffuse to the dot surface and grow in size. The standard synthesis is as follows.

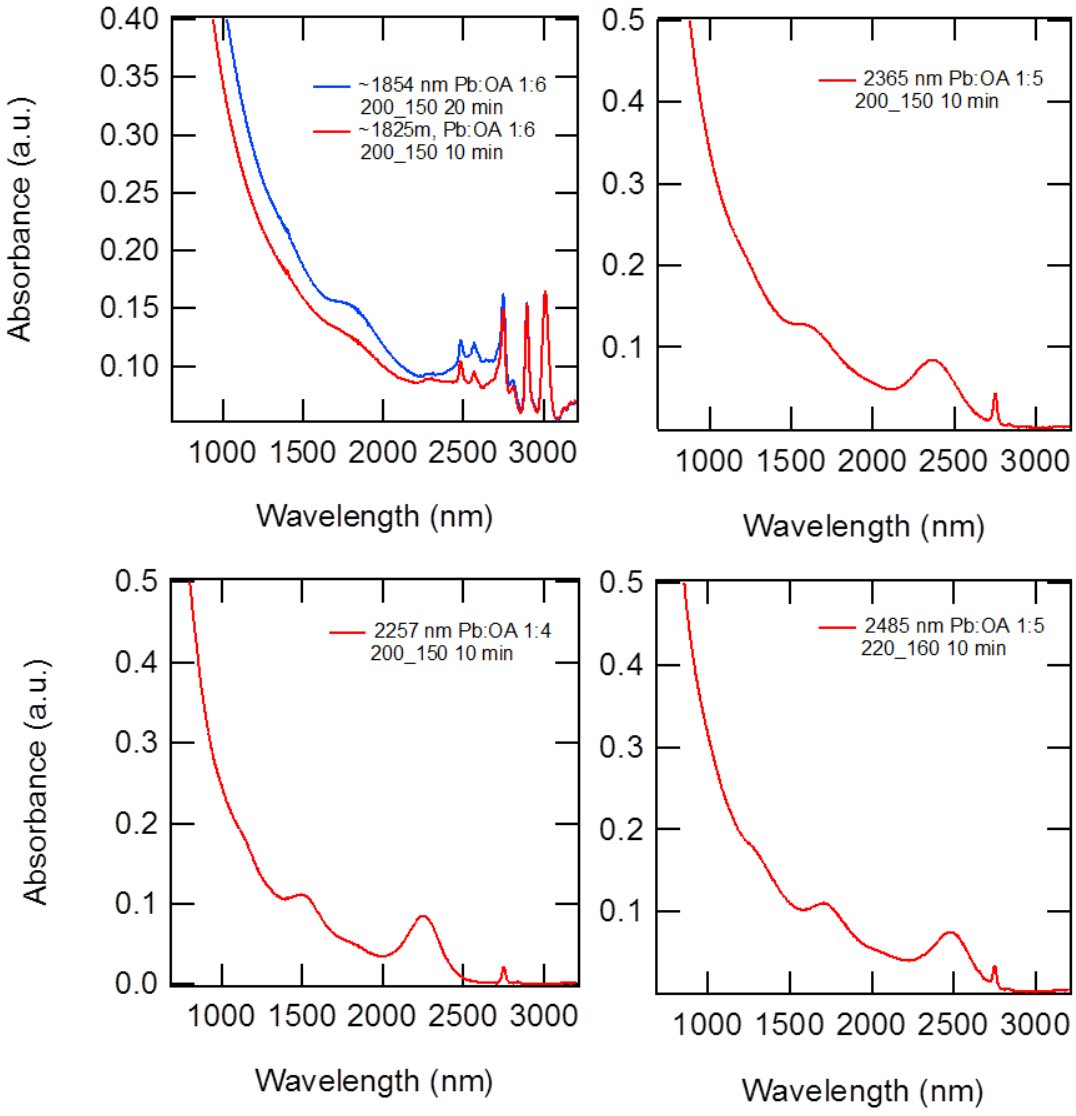

Figure 33. UV-vis spectra demonstrating synthesis parameter adjustment to create ~2500 nm PbSe

Synthesis of 11.5 nm PbSe Nanocrystals:

The large PbSe QDs were synthesized and purified using standard air-free techniques. PbO (1.09 g), OA (5.51 g), and ODE (11.20 g) were mixed and degassed in a three-neck round-bottom flask at room temperature. Then, the mixture was heated at 120°C under vacuum to dissolve the PbO and dry the solution. After 1 hour, the Pb(OA)2 solution was heated to 220°C under argon flow. 15 mL of a 1 M solution of TOP-Se containing 130 µL of DPP (0.75 mmol) was then rapidly injected into this hot solution. The temperature controller was then set to 160°C and the QDs were grown for 10 min at 160°C. The reaction was quenched with a liquid nitrogen bath and injection of 15 mL of anhydrous hexane. The QDs were purified by three rounds of precipitation/redispersion using ethanol/hexane and stored as a powder in a glovebox.

As shown in Figure 34, this synthesis was very reproducible and an unexpected result was that the nanocrystals were cubic. When PbX nanocrystals nucleate, the (111) facets are most dominate. As the nanocrystals grow the (100) facets become more apparent and the (111) facets reduce in surface area on the nanocrystal. The cubes produced here have (100) as the dominant facets, but from TEM images, the (111) facets can still be seen, although quite small.

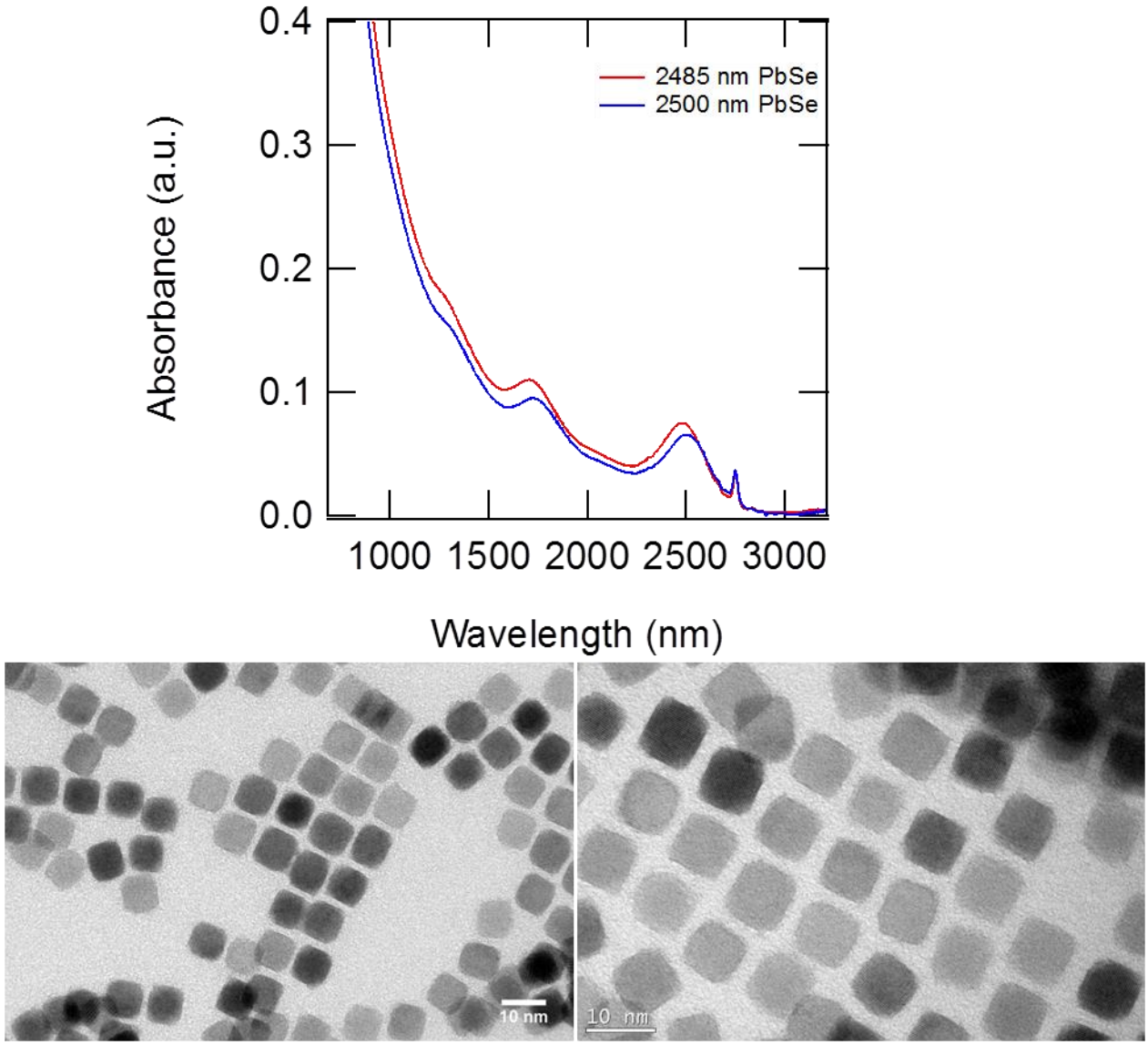

Figure 34. (Top) Absorption spectra of large PbSe QDs, demonstrating reproducibility. (Bottom) TEM micrographs of 11.57 ± 0.52 nm PbSe cubes (size was measured across diagonal of cube)

It was found that the QD purification step played an important part in devices. By increasing the number of washed from 2 to 3, photoresponsivity drastically improved as shown in Figure 35. The most likely reason for the device improvements is that 2 washes did not remove all of the unreacted precursors from the synthesis and were electronically or optically

insulating the nanocrystals. Another reason could be that the additional washing step slightly stripped some oleate ligand creating trap states that could prove beneficial when interacting with other interfaces.

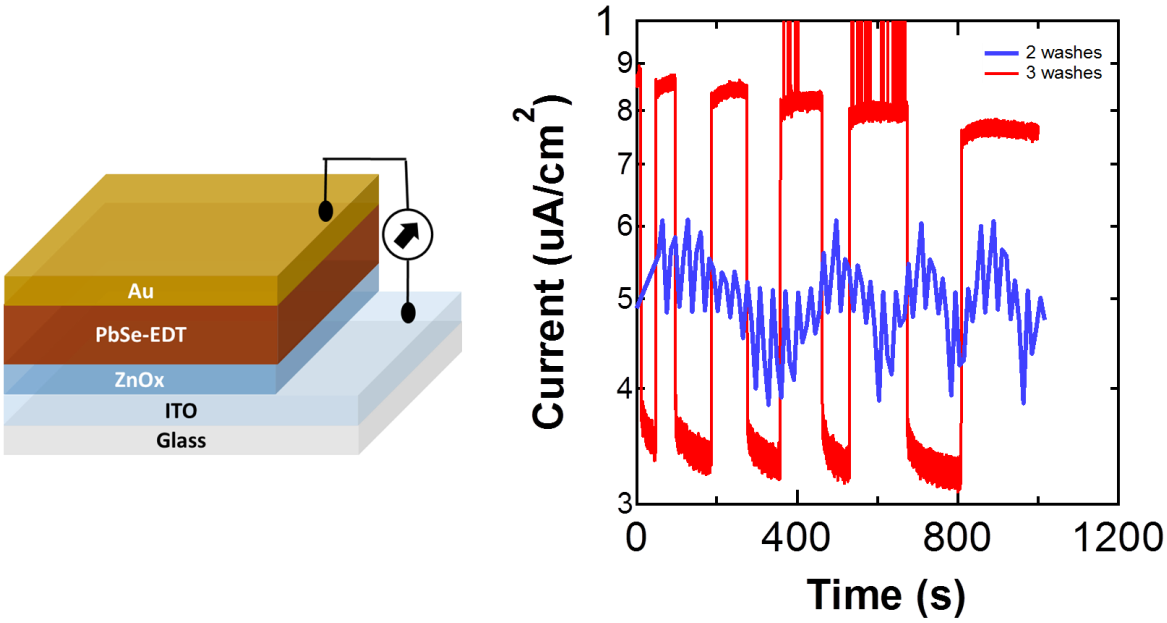

Figure 35. Effect of Washing on the photoresponsivity of PbSe-EDT devices

The large PbSe cubes synthesized during the course of this thesis were used to produce several batches of devices, fabricated by Chao Yi. Through several trials, it found that by partial ALD infilling the ZnO layer of the devices with amorphous TiO_2 surface trap states or mid-gap states were removed dramatically improving device performance (Figure 36). This led to record performance with the best devices achieving a detectivity of over 10^{12} Jones.

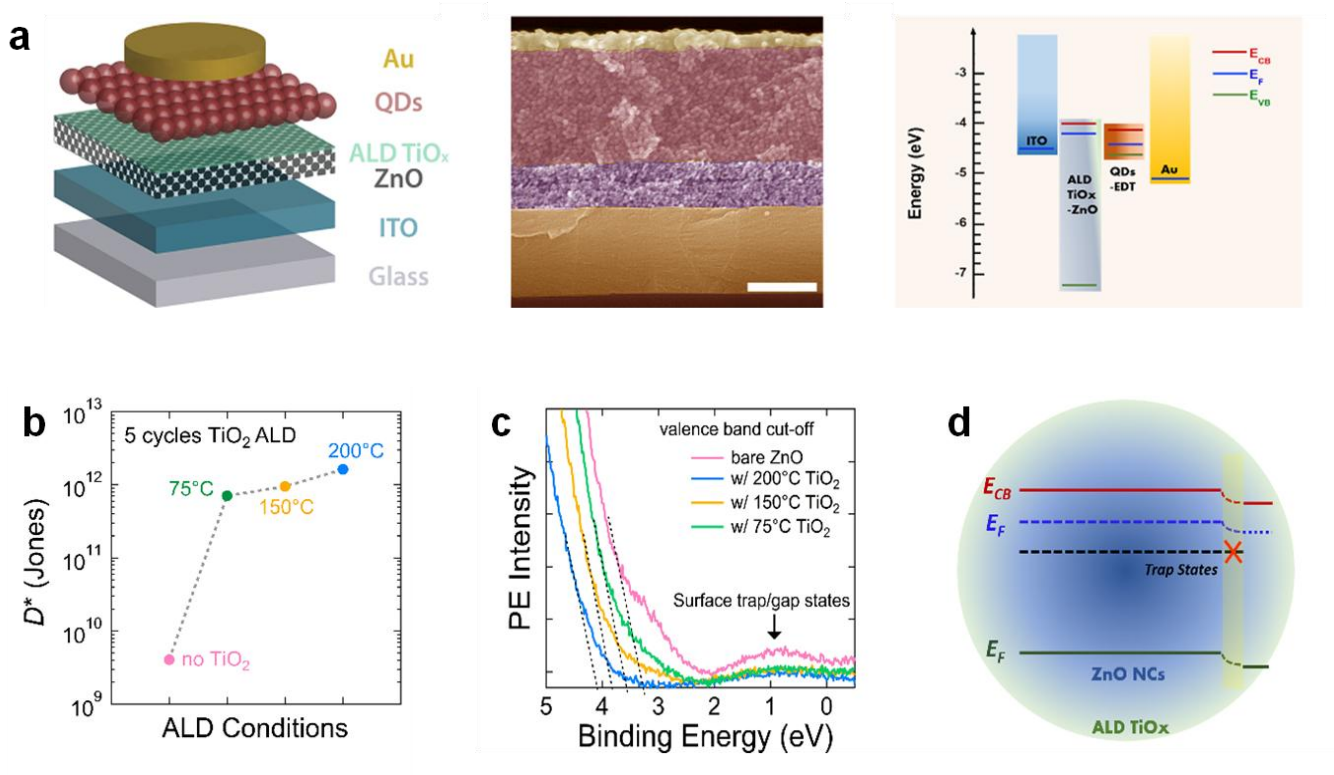

Figure 36. Photodetector utilizing large PbSe cubes. Data courtesy of Chao Yi. a. Photodetector architecture and relative band positions. b. TiO_2 ALD conditions to improve device performance. c and d. UPS spectra and illustration of surface trap/gap state removal using TiO_2 ALD.

Conclusion and Future Work

Conclusion

The focus of this thesis was to provide a better understanding of PbTe QDs and determine if they are a worthwhile material to improve charge transport in FETs, photodetectors, or solar cells. In theory, this material should have better electronic coupling and higher mobilities than PbSe QDs based on its large dielectric constant and Bohr exciton radius. This is hindered by the fact that PbTe QDs oxidize very rapidly, as verified by UV-VIS and XPS experiments, and it is currently impossible to create a stable device from the material that can operate outside a glovebox. These studies demonstrate the effectiveness of ALD infilled PbTe FETs to negate oxidative degradation through measurements of the stability and electrical properties over the long term with thiol surface chemistries. As the ALD treatment passivates surface trap states, n-channel FET devices were created, demonstrating 1.8 $cm^2/V{\cdot}s$ electron mobility. PbTe and PbSe QDs of various sizes were successfully synthesized with good monodispersity by adjusting concentration of precursors, growth time, and temperature. Large PbSe cubes were implemented in photodetector devices to create record performance detectivities.

Future Work

Due to the sensitive nature of PbTe QDs, many of these results need to be repeated before publication as the electronic properties can easily be affected by small amounts of oxygen and solvent environments in nitrogen filled gloveboxes that have fluctuated during the experiments thus far. In addition, due to the limited literature resources on PbTe QDs, experiments involving PbTe QDs and ALD will become novel, original work. The following are proposed tasks to further this project

1) Further assess the environmental stability of PbTe QDs in films relative to PbSe QDs. Evaluate the effectiveness of ALD infilling for stabilizing films. Determine impact of unintentional oxidation on film electronic properties and develop countermeasures to access the intrinsic electrical properties.

    -Utilize the XPS and oxygen dosing to determine what species form when PbTe and PbSe are oxidized and at what rate/oxygen dosage.

    -Use other ALD infilling materials such as ZnO that may have a stronger influence on passivation and doping PbTe QDs. This is because all FET behavior with no ALD treatments thus far and some alumina infilled devices, are always p-channel devices (hole conducting), regardless of what surface chemistry that is used on this material. If unable to access the intrinsic properties, this may be an alternative to compensate/dope the strong p-channel character of the material

2) Determine whether and why/why not PbTe films have better charge transport properties than PbSe films. Evaluate the hypothesis that the larger Bohr exciton radius of PbTe leads to better coupling and higher mobility than PbSe QDs.

This task has remained difficult to tackle as PbTe QDs always have presented with electronic, optical, or structural characteristics that have made it inferior to PbSe thus far when using small conductive ligands. It would be best to utilize a colloidal ALD route to somehow passivate and grow a thin shell of oxide or another semiconductor on the PbTe QDs while they still have their native ligands. This could make it feasible to evaluate PbTe and compare it to PbSe since the QD surface would be protected from oxidation before ligand exchange occurs.

3) Making and measuring PbTe QDs solar cells to evaluate MEG and slower hot carrier cooling steps relative to PbSe and PbS solar cells

-Ideally, make a photodiode using ~5nm PbTe QDs to serve as a baseline in an air-free environment. If successful, will need a way to incorporate the ALD infilling to prevent oxidation to PbTe QDs while still allowing for good charge transport.

-To evaluate MEG, PbTe and PbSe samples could be examined using time-resolved microwave conductivity measurements that can measure free charge generation by monitoring the absorption of microwave radiation with respect to time.

4) Creating a new synthesis to make high yield, monodisperse PbTe QDs.

Due to PbTe's reactivity, conventional nucleation assisting precursors such as diphenylphosphine are too reactive and cause loss of nanocrystal growth control and produce particles too large to remain colloidally suspended.

Other countermeasures should also be explored to improve or hinder oxidation by applying strong reducing agents to films or utilizing core-shell approaches to improve surface passivation before the QDs are incorporated into a film. It will be determined if these surface and matrix engineering methods can be incorporated into working PV devices and if S-Q limit can indeed be surpassed through improved MEG processes.

References

[1] International energy outlook, U.S. energy information administration, 2017

[2] O. Morton, "A task of terawatts", Nature Collections Energy, https://www.nature.com/nature/supplements/collections/energy/editorial.pdf

[3] K.W. Johnston, A. G. Pattantyus-Abraham, J.P.Clifford, et al., "Efficient Schottky-quantum-dot photovoltaics: The role of depletion, drift, and diffusion. Applied Physics Letters, 2008, 92, 122111

[4] A. Polman, M. Knight, E. C. Garnett, B. Ehrler, W. C. Sinke, Photovoltaic materials: Present efficiencies and future challenges, Science, 2016, 352, 15

[5] G. Colinbeer, "Third Generation Photovoltaics," Materials Today, 2007, 10, 42-50

[6] T. D. Lee, A.U. Ebong, "A review of thin film solar cell technologies and challenges," Renewable and Sustainable Energy Reviews, 2017, 70, 1286

[7] N.Alia, A.Hussain, R.Ahmed, M.K.Wang, C. Zhao, B. Ul Haq, Y.Q.Fud, "Advances in nanostructured thin film materials for solar cell applications," Renewable and Sustainable Energy Reviews, 2016, 59, 726

[8] NREL, National center for photovoltaics: http://www.nrel.gov/ncpv/

[9] F.W. Wise, “Lead Salt Quantum Dots: the Limit of Strong Quantum Confinement,” Acc. Chem. Res., 2000, 33, 773-780

[10] J. E. Murphy, M.C. Beard, A.G, Norman, S.P. Ahrenkiel, J.C. Johnson, P. Yu., O. Micic, R.J. Ellingson, A.J. Nozik, “PbTe Colloidal Nanocrystals: Synthesis, Characterization, and Multiple Exciton Generation,” J. Am. Chem. Soc. 2006, 128, 3241-3247

[11] E.H. Sargent, G. Konstantatos, “Colloidal Quantum Dot Optoelectronics and Photovoltaics”, Cambridge University Press, 2013

[12] S. ten Cate, C.S.S. Sandeep, Y. Liu, M. Law, S. Kinge, A.J. Houtepen, J.M. Schins, L.D.A. Siebbeles, “Generating free charges by carrier multiplication in quantum dots for highly-efficient photovoltaics,” Acct. Chem. Res., 2015, 48, 174-181

[13] J. T. Stewart, L. A. Padilha, W. Bae, W. K. Koh, J. Pietryga, V. I. Klimov, “Carrier Multiplication in Quantum Dots within a Framework of Two Competing Energy Relaxation Mechanisms,” J. Phys. Chem., 2013, 4, 2061-2068

[14] M. L. Böhm, T. C. Jellicoe, M. Tabachnyk, N. J. L. K. Davis, F. Wisnivesky-Rocca-Rivarola, C. Ducati, B. Ehrler, A. A. Bakulin, and N. C. Greenham, “ Lead Telluride Quantum Dot Solar Cells Displaying External Quantum Efficiencies Exceeding 120%,” Nano Lett., 2015, 15, 7987–7993

[15] C. B. Murray, D. J. Norris, M. G. Bawendi, “Synthesis and characterization of nearly monodisperse CdE (E = sulfur, selenium, tellurium) semiconductor nanocrystallites” Journal of the American Chemical Society, 1993, 115, 8706–8715.

[16] C. B. Murray, C. R. Kagan , M. G. Bawendi , “Synthesis and characterization of monodisperse nanocrystals and close-packed nanocrystal assemblies,” Annual Review of Materials Science, 2000, 30, 545–610.

[17] H. Zhang, J. Jang, W. Liu, D.V. Talapin, "Colloidal Nanocrystals with Inorganic Halides, Pseudohalide, and Halometallate Ligands," ACS Nano, 2014 8, 7359-7369

[18] J. Zhang, J. Gao, E.M. Miller, J.M. Luther, M.C. Beard, "Diffusion Controlled Synthesis of PbS and PbSe Quantum Dots with in Situ Halide Passivation for Quantum Dot Solar Cells," ACS Nano, 2013, 8, 614-622.

[19] I. Gur, N.A. Fromer, M. L.Geier, A.P. Alivisatos, "Air-Stable All-Inorganic Nanocrystal Solar Cells Processed from Solution," Science, 2005, 310, 462– 465

[20] H. Fang, H. Yang, Y. Wu, " Thermoelectric Properties of Silver Telluride–Bismuth Telluride Nanowire Heterostructure Synthesized by Site-Selective Conversion," Chem. Mater. 2014, 26, 3322– 3327

[21] M. Scheele, N. Oeschler, I. Veremchuk, S.O. Peters, A. Littig, A. Kornowski, C. Klinke, H. Weller, " Thermoelectric Properties of Lead Chalcogenide Core–Shell Nanostructures" ACS Nano 2011, 5, 8541– 8551

[22] K. S. Leschkies, T.J. Beatty, M. S., Kang, D. J. Norris, E. S. Aydil, "Solar Cells Based on Junctions between Colloidal PbSe Nanocrystals and Thin ZnO Films" ACS Nano, 2009, 3, 3638– 3648

[23] A.T. Fafarman, W.K. Koh, B.T. Diroll, D. K. Kim, D. K. Ko, S. J. Oh, X, Ye, V. Doan-Nguyen, M.R. Crump, D.C. Reifsnyder, C.B. Murray, C.R. Kagan, " Thiocyanate-Capped Nanocrystal Colloids: Vibrational Reporter of Surface Chemistry and Solution-Based Route to Enhanced Coupling in Nanocrystal Solids," J. Am. Chem. Soc. 2011, 133, 15753– 15761

[24] D. N. Dirin, S. Dreyfuss, M.I. Bodnarchuk, G. Nedelcu, P. Papagiorgis, G. Itskos, M.V. Kovalenko, "Lead Halide Perovskites and Other Metal Halide Complexes As Inorganic Capping Ligands for Colloidal Nanocrystals," J. Am. Chem. Soc. 2014, 136, 6550– 6553

[25] A. Nag, M.V. Kovalenko, J.S. Lee, W. Liu, B. Spokoyny, D. V. Talapin, "Metal-free Inorganic Ligands for Colloidal Nanocrystals: S2–, HS–, Se2–, HSe–, Te2–, HTe–, TeS32–, OH–, and NH2– as Surface Ligands," J. Am. Chem. Soc. 2011, 133, 10612– 10620

[26] A. Stavrinadis, G. Konstantatos, "Strategies for the Controlled Electronic Doping of Colloidal Quantum Dot Solids" ChemPhysChem 2016, 17, 632– 644

[27] Y. Liu, J. Tolentino, M. Gibbs, R. Ihly, C.L. Perkins, Y. Liu, N. Crawford, J.C. Hemminger, M. Law, " PbSe quantum dot field-effect transistors with air-stable electron mobilities above 7 cm2 V-1 s-1," Nano Letters, 2013, 13, 1578-1587

[28] J.J. Urban, D. V. Talapin, E. V. Shevchenko, C. B. Murray, "Self Assembly of PbTe Quantum Dots into Nanocrystal Superlattices and Glassy Films," J. Am. Chem. Soc., 2006, 128, 3248-3255.

[29] Voznyy, O.; Zhitomirsky, D.; Stadler, P.; Ning, Z.; Hoogland, S.; Sargent, E. H., A charge-orbital balance picture of doping in colloidal quantum dot solids. ACS Nano., 2012, 6 (9), 8448-55.

[30] Tolentino, J., "Designing quantum dot solid for optoelectronic devices through matrix Engineering," Ph.D. Dissertation, University of California, Irvine, Irvine, CA, 2015.

[31] Gibbs, M. L., "Construction and Analysis of PbSe Quantum Dot Heterojunction Solar Cells," Ph.D. Dissertation, University of California, Irvine, Irvine, CA, 2014.

[32] Ihly, R., "Quantum Dot heterojunction solar cells: the mechanism of device operation and impacts of quantum dot oxidation," Ph.D. Dissertation, University of California, Irvine, Irvine, CA, 2014.

[33] Groner, M. D.; Fabreguette, F. H.; Elam, J. W.; George, S. M. "Low-Temperature Al2O3 Atomic Layer Deposition." Chem. Mater. 2004, 16, 639–45.

[34] Valdesueiro, D.; Prabhu, M. K.; Guerra-Nunez, C.; Suchand Sandeep, C.S.; Kinge, S.; Siebbeles, L.; de Smet, L.; Meesters, G.; Kreutzer, M.; Houtepen, A.; Ruud van Ommen, J. "Deposition Mechanism of Aluminum Oxide on Quantum Dot Films at Atmospheric Pressure and Room Temperature." J. Phys. Chem. C., 120, 8, 4266-4275